Histochemistry and Cell Biology (2023) 159:127–147
https://doi.org/10.1007/s00418-022-02157-2

ORIGINAL PAPER

Increased double-strand breaks in aged mouse male germ cells may result from changed expression of the genes essential for homologous recombination or nonhomologous end joining repair

Gunel Talibova[1] · Yesim Bilmez[1] · Saffet Ozturk[1]

Accepted: 27 September 2022 / Published online: 15 October 2022

Abstract
DNA double-strand breaks (DSBs) are commonly appearing deleterious DNA damages, which progressively increase in male germ cells during biological aging. There are two main pathways for repairing DSBs: homologous recombination (HR) and classical nonhomologous end joining (cNHEJ). Knockout and functional studies revealed that, while RAD51 and RPA70 proteins are indispensable for HR-based repair, KU80 and XRCC4 are the key proteins in cNHEJ repair. As is known, γH2AX contributes to these pathways through recruiting repair-related proteins to damaged site. The underlying reasons of increased DSBs in male germ cells during aging are not fully addressed yet. In this study, we aimed to analyze the spatiotemporal expression of the *Rad51*, *Rpa70*, *Ku80*, and *Xrcc4* genes in the postnatal mouse testes, classified into young, prepubertal, pubertal, postpubertal, and aged groups according to their reproductive features and histological structures. We found that expression of these genes significantly decreased in the aged group compared with the other groups ($P < 0.05$). γH2AX staining showed that DSB levels in the germ cells from spermatogonia to elongated spermatids as well as in the Sertoli cells remarkably increased in the aged group ($P < 0.05$). The RAD51, RPA70, KU80, and XRCC4 protein levels exhibited predominant changes in the germ and Sertoli cells among groups ($P < 0.05$). These findings suggest that altered expression of the *Rad51*, *Rpa70*, *Ku80*, and *Xrcc4* genes in the germ and Sertoli cells may be associated with increasing DSBs during biological aging, which might result in fertility loss.

Keywords DNA double-strand break (DSB) · HR repair · cNHEJ repair · Male germ cells · Testicular aging · Fertility loss

Introduction

Male infertility is a widespread reproductive problem, and 40–60% of infertility among couples originates from male factors (Esteves et al. 2011; Ji et al. 2012). Approximately 30% of male factor-induced infertility is not fully addressed yet (Duca et al. 2019). DNA damages, especially DNA double-strand breaks (DSBs) occurring in germ cells during spermatogenesis (Gunes et al. 2015; Agarwal et al. 2020), may underlie development of idiopathic male infertility. DSBs can arise from ionizing radiation, chemotherapeutic drugs, defective chromatin packaging, incomplete apoptosis, oxidative damage, and replication errors (Khanna and Jackson 2001). Many mitotic divisions in spermatogonial cells and meiotic recombination in spermatocytes may result in formation of the DSBs, which must be repaired in a timely and accurate manner (Tesarik et al. 2004; Gonzalez-Marin et al. 2012). If DSBs remain unrepaired, various chromosomal rearrangements and genetic mutations may emerge in the resulting sperm cells (Cortes-Gutierrez et al. 2014). Fertilization of mature oocytes with these sperm cells can lead to production of the embryos showing genomic instability, developmental delay, increased cell death, and reduced viability (Fernandez-Gonzalez et al. 2008; Her and Bunting 2018). To avoid these unfavorable outcomes, DSBs are efficiently repaired in male germ cells by two main pathways: homologous recombination (HR) and classical/canonical nonhomologous end joining (cNHEJ) (Grabarz et al. 2012; Talibova et al. 2022). It is noteworthy that other DSB repair pathways, such as alternative end joining (aEJ) and single-strand annealing (SSA), also contribute to repair of DSBs in

✉ Saffet Ozturk
sozturk@akdeniz.edu.tr

[1] Department of Histology and Embryology, Akdeniz University School of Medicine, Campus, 07070 Antalya, Turkey

some circumstances, e.g., in the absence of cNHEJ pathway (Scully et al. 2019).

The first step of repairing DSBs is the introduction of damaged sites. Histone H2A variant (H2AX) contributes to marking these sites (Kinner et al. 2008). In this case, serine 139 of conserved C-terminal tail of H2AX is phosphorylated by DNA-dependent protein kinase (DNA-PK) (Yuan et al. 2010). One of the two pathways (HR or cNHEJ) is activated on the basis of cell cycle status or abundance of repair-related proteins in the microenvironment. In the cNHEJ pathway (Pannunzio et al. 2018), minimal end processing and base pairing occur at the broken DNA ends. After expanding chromatin in the vicinity of breaks by the action of poly(ADP-ribose) polymerase 1 (PARP1) and ATP-dependent chromatin remodelers (Sellou et al. 2016), the KU70-KU80 heterodimer (also known as XRCC6–XRCC5) binds DNA to initiate repair. This heterodimer recruits the DNA-dependent protein kinase catalytic subunit (DNA-PKcs), DNA ligase IV (LIG4), and the scaffold factors, including XRCC4-like factor (XLF) and paralog of XRCC4 and XLF (PAXX) (Gottlieb and Jackson 1993; Ahnesorg et al. 2006). Meanwhile, X-ray repair cross-complementing protein 4 (XRCC4) ensures stability and activity of LIG4 (Grawunder et al. 1997; Pandey and Raghavan 2017). Ultimately, the end-processing enzymes, Artemis as a nuclease and DNA polymerase λ/μ, and accessory proteins accomplish ligation of the free DNA ends (Stinson et al. 2020).

The *Ku80* gene is expressed in spermatogonia, spermatocytes at late pachytene and diplotene stages, and Sertoli cells in mouse testes (Ahmed et al. 2007). Its loss caused premature cellular senescence, growth retardation (Ouyang et al. 1997), and shortened lifespan in mice (Lombard et al. 2005). Lacking another key cNHEJ component *Xrcc4* led to embryonic lethality probably because of accumulation of unrepaired DSBs during early development (Gao et al. 2000; Li et al. 2016a). Also, XRCC4-deficient embryonic fibroblasts showed genomic instability such as translocations among chromosomes. Taken together, KU80 and XRCC4 play crucial roles in successfully repairing DSBs in male germ cells and embryos.

HR-based DSB repair is dependent on using sister or non-sister chromatid of homologous chromosomes as a template (Sung and Klein 2006). RAD51 is a critical protein in HR repair initiation, in which it establishes an interaction between single-strand DNA (ssDNA) and duplex DNA, and thereby promotes strand exchange (Sung et al. 2003; Li and Heyer 2008). When *Rad51* is knocked out, prophase I spermatocytes were depleted owing to dramatically increased apoptosis (Dai et al. 2017). Another key protein in HR repair, replication protein A 70 (RPA70), interacts with ssDNA after free ends were created (Iftode et al. 1999). Thus, RPA70 comprises a filament on ssDNA to hamper formation of secondary structures (Chang et al. 2017). Failure to form an RPA complex in mouse primary spermatocytes resulted in the accumulation of DSBs and considerable reduction of crossing-over (Shi et al. 2019).

DSB repair efficiency gradually declines with biological aging, which results in the increase of DSBs (Vaidya et al. 2014; Li et al. 2016b). Consistently, DSB levels in sperm cells of older individuals (aged 36–57 years old) were significantly higher than those from young individuals (20–35 years old) (Singh et al. 2003) as similarly revealed in a recent study (Rosiak-Gill et al. 2019). As a result, DNA damage, especially DSBs, gradually increases in men during aging, accompanied by fertility loss. The underlying reasons for increased DSBs in sperm cells during aging are not fully understood yet. We hypothesized in the present study that changed expression of the HR and cNHEJ genes in male germ cells during aging may underlie the accumulation of DSBs. For this purpose, we have evaluated the spatiotemporal expression of the *Rad51*, *Rpa70*, *Ku80*, and *Xrcc4* genes as well as γH2AX distribution in the postnatal mouse testes from young to aged periods.

Materials and methods

Animals and sample collection

BALB/c male mice aged 1, 2, 3, 4, 5, 6, 16, 18, 20, 48, 50, and 52 weeks were used in this study. The five groups were created on the basis of histological structures and reproductive features as follows: young (1 and 2 weeks old; $n = 5$ from each week), prepubertal (3 and 4 weeks old; $n = 4$ from each week), pubertal (5 and 6 weeks old; $n = 4$ from each week), postpubertal (16, 18, and 20 weeks old; $n = 4$ from each week), and aged (48, 50, and 52 weeks old; $n = 6$, 5, and 6 from each week, respectively). We provided these mice from Akdeniz University Experimental Animals Application and Research Center, and they were kept under a 12 h light–dark cycle without water and food restrictions. All experimental protocols were carried out in accordance with the relevant guidelines and regulations approved by the Akdeniz University Institutional Animal Care and Use Committee (protocol number 937/2019.07.10). Following cervical dislocation, which was carried out immediately after ether inhalation, we dissected testes from each mouse under sterile conditions using a stereo microscope (Zeiss, Oberkochen, Germany). One testis from each mouse was used for quantitative real-time polymerase chain reaction (qRT-PCR), and the other one underwent routine paraffin embedding for hematoxylin and eosin (HE) and immunohistochemistry staining.

Gene expression analysis

Rad51, *Rpa70*, *Ku80*, and *Xrcc4* gene expression analysis in the postnatal testes was carried out by qRT-PCR as in previous studies (Bustin et al. 2009; Ozturk et al. 2012, 2014; Kosebent and Ozturk 2021a). Total RNA was isolated using TRIzol reagent (Life Technologies, Darmstadt, Germany) according to the manufacturer's instructions and kept at −80 °C until use. The concentration and absorbance values of isolated RNA were determined by measuring at the wavelengths of 260 and 280 nm using the Epoch microplate spectrophotometer (BioTek, Winooski, VT, USA). Ten micrograms of extracted RNA was treated with DNase I (Ambion, Austin, Texas, USA) to eliminate any genomic DNA contamination. We subsequently generated complementary DNA (cDNA) from 2 µg of DNAase I-treated RNA in a 20 µl reverse-transcriptase reaction using the RETROscript kit (Ambion, Austin, TX, USA) according to the instructions supplied by the manufacturer. For this reaction, we used 100 units of M-MLV reverse transcriptase enzyme. Finally, the reaction tubes were incubated at 42 °C for 60 min and then 95 °C for 10 min.

The relative mRNA levels of the *Rad51* (RefSeq accession number NM_011234.5), *Rpa70* (RefSeq accession number NM_001252415.2), *Ku80* (RefSeq accession number XM_006495893.4), and *Xrcc4* (RefSeq accession number NM_028012.4) genes were detected by qRT-PCR in a total volume of 25 µl composed of 12.5 µl of 2× SYBR Green Supermix (Bio-Rad, Hercules, California, USA), 10 µM of primers, and 1 µl of 1:10 diluted cDNA. The primer sequences and product sizes are given in Table 1. All primer sequences were selected according to the literature studies, which were also confirmed using the Primer-BLAST program (https://www.ncbi.nlm.nih.gov/tools/primer-blast/). Amplifications were carried out with 35 cycles as follows: 95 °C for 15 min (initial denaturation), for 10 cycles: 92 °C for 20 s, 67 °C for 20 s, and 72 °C for 60 s (acquired to Cycling A Green), and 25 cycles: 92 °C for 20 s, 55 °C for 15 s, and 72 °C for 60 s (acquired to Cycling A Green), and final extension at 72 °C for 60 s. In the end, melting curve analysis (55–95 °C for 5 s each) was performed to confirm specificity of the PCR products. PCR cycling was applied in triplicate on a Rotor-Gene (Corbett Research, Sydney, Australia). *β-Actin* was used as a reference gene to normalize relative mRNA levels of the target genes. The $2^{-\Delta\Delta Cq}$ (where Cq stands for quantification cycle) formula was utilized to calculate fold changes. Thus, relative *Rad51*, *Rpa70*, *Ku80*, and *Xrcc4* expression levels were determined in the postnatal testes from young to aged groups.

Table 1 The primer sequences and product sizes of the *β-Actin*, *Rad51*, *Rpa70*, *Ku80*, and *Xrcc4* genes used in qRT-PCR. *bp* base pair

Gene	Primers (5′ → 3′)	Product size (bp)
β-Actin	Forward: TGCGTGACATCAAAGAGAAG Reverse: CGGATGTCAACGTCACACTT	244
Rad51	Forward: AAACCTGACAGAGGAGCAGC Reverse: TGCATAAGCAACAGCCTCCA	278
Rpa70	Forward: TGGGCTTCTTTGCAGTCTGT Reverse: CGGGTGAGTGAACAGGGATG	292
Ku80	Forward: CTTGCTGGCAAGGACCAGTA Reverse: GGAAGGAGGGTTTGAGGTGG	376
Xrcc4	Forward: CGCAAGTGGAGTACTGAGAGG Reverse: ATGTACCAGCTGCTCCTGAC	280

Paraffin embedding

Paraffin-embedded tissue processing was performed as in our previous studies (Ozturk et al. 2012; Tepekoy et al. 2015). The testes obtained from 1-, 2-, 3-, 4-, 5-, 6-, 16-18-, 20-, 48-, 50-, and 52-week-old mice were immersed in Bouin's solution at +4 °C for 24 h. Then, they were dehydrated in increasing concentrations of ethanol, cleared in xylene, and subsequently embedded in paraffin. The paraffin blocks were cut serially at 5 µm thickness using a rotary microtome (Leica, Nussloch, Germany). We used these sections mounted onto Superfrost Plus glass slides (Thermo Scientific, Rockford, IL, USA) in the following analyses.

Histological analysis

HE staining of the sections was carried out not only to evaluate the histological structure of the postnatal testes but also to count the germ cells from spermatogonia to elongated spermatids as well as Sertoli cells. In brief, we incubated sections in an oven at 60 °C for 1 h for HE staining. After that, sections were treated twice with xylene for 10 min each time, and then rehydrated in the decreasing ethanol concentrations for 5 min each time. After washing sections under tap water, we stained them with hematoxylin followed by eosin. Eventually, the histological structure of the postnatal testes was evaluated under a bright-field microscope (Carl Zeiss Inc., Thornwood, NY, USA).

For cell counting, we identified germ and Sertoli cells on the basis of their well-defined morphological characteristics (Kotaja et al. 2004; Gribbins et al. 2006; Ozturk et al. 2012, 2014). Spermatogonial cells located at the basal site of seminiferous tubules were distinguished by a deeply stained nucleus surrounded with a rim of cytoplasm. Primary spermatocytes were counted in two subgroups as early prophase (including preleptotene, leptotene and zygotene stages) and pachytene. While preleptotene spermatocytes possessed a prominent nucleus and fine granular chromatin, the leptotene spermatocytes were in slightly larger diameter, stained more

intensely, and had a fine filamentous chromatin packed in their nuclei. We distinguished zygotene spermatocytes as having a large size and thickened filamentous chromatin fibers within nucleus. Pachytene spermatocytes are the largest among germ cells and contain very thick chromatin fibers, which are interspersed in the nucleoplasm.

We defined round spermatids at steps 1–8 by the round nucleus including a centrally localized nucleolus (Meistrich and Hess 2013; O'Donnell 2014). While elongating spermatids at steps 9–11 locating close to seminiferous tubule lumen had an oval nucleus and no flagella, the elongated ones at steps 12–16 were recognized by their hook-shaped nucleus, surrounded by a small amount of cytoplasm, and presence of a flagella (Meistrich and Hess 2013; Fu et al. 2018). Sertoli cells, the largest somatic cell of seminiferous tubules, were defined as having round-, oval-, or irregular-shaped nucleus with a centrally located nucleolus (Meistrich et al. 1973; Vasco et al. 2009). On the basis of the characteristics of these cells, randomly selected ten seminiferous tubules in each testis section from each mouse at the ages of 1, 2, 3, 4, 5, 6, 16, 18, 20, 48, 50, and 52 weeks were assessed by two independent researchers under a bright-field light microscope (Optiphot 300, Nikon, Japan). The number of germ and Sertoli cells per seminiferous tubule was determined.

Immunohistochemical staining

We performed immunohistochemical staining as in our previous studies (Uysal and Ozturk 2020; Kosebent and Ozturk 2021b) to determine the spatiotemporal distributions and relative abundances of the γH_2AX, RAD51, RPA70, KU80, and XRCC4 proteins in the postnatal testes. The sections cut from the paraffin-embedded blocks were deparaffinized in fresh xylene after being held in an oven at 60 °C for 1 h and then rehydrated in a decreasing ethanol series. We boiled sections in Tris–EDTA solution (including 10 mM Tris base and 1 mM EDTA) in a microwave, set at 665 W for 5 min, for antigen retrieval. Subsequently, endogenous peroxidase activity was blocked in 3% H_2O_2 solution (prepared in methanol) for 25 min at room temperature (RT). After washing with phosphate-buffered saline (1× PBS), sections were blocked by incubating with Ultra V blocking solution at RT for 7 min to prevent nonspecific binding.

Afterward, we incubated the sections with the γH_2AX (diluted 1:1500, catalog no. 9718S, Cell Signaling), RAD51 (diluted 1:500, catalog no. bs-20297R, Bioss), RPA70 (diluted 1:1750, catalog no. ab12320, Abcam), KU80 (diluted 1:750, catalog no. MBS712948, MyBiosource), and XRCC4 (diluted 1:750, catalog no. bs8510R, Bioss) primary antibodies at + 4 °C overnight. All these primary antibodies were produced in rabbits. Importantly, isotype IgG antibody (diluted at the same concentrations with the primary antibodies, catalog no. I5006, Sigma-Aldrich) except for the RAD51 immunostaining (in which we used 1× PBS solution instead of primary antibody) was employed in staining negative-control sections to detect specificity of the primary antibodies. Following primary antibody incubation, sections were washed in PBS for 15 min three times and then incubated with biotinylated secondary antibody (goat anti-rabbit IgG, diluted 1:750, catalog no. BA-1000, Vector Labs) for 1 h at RT. Sections were then treated with streptavidin–horseradish peroxidase (HRP) complex (catalog no. TS-125-HR, Thermo Scientific) for 30 min at RT. Finally, the immunoreactions were revealed using 3, 3′-diaminobenzidine (DAB) substrate (catalog no. D4168, Sigma-Aldrich) under a light microscope. After washing sections under running tap water, we counterstained them with Mayer's hematoxylin for visualization of nuclei.

The spatiotemporal distributions and relative levels of the γH_2AX, RAD51, RPA70, KU80, and XRCC4 proteins in total, per seminiferous tubule, and in each germ and Sertoli cell type were evaluated in the postnatal testes from young to aged groups using the ImageJ software program [National Institutes of Health (NIH), Bethesda, Maryland, USA]. For this purpose, the micrographs were captured under a Zeiss bright-field microscope with Axiocam 105 color at 200× original magnification. The integrated mean values measured by the ImageJ software program were divided into area values to determine unit expression levels. It is worth noting that we analyzed at least four images from each age.

Statistical analysis

The obtained data were evaluated using one-way analysis of variance (one-way ANOVA) on ranks, followed by a suitable post hoc test. We conducted all statistical calculations using GraphPad Prism 5. $P < 0.05$ was considered statistically significant.

Results

Histological analysis and cell counting

In this study, we first evaluated the histological structure of the postnatal mouse testes from 1 to 52 weeks of age, whose representative micrographs are shown in Fig. 1a. In the young group, only spermatogonia and Sertoli cells were observed in 1-week-old testis, and a low number of primary spermatocytes at early prophase or pachytene stage were observed in 2-week-old testis. In addition to the primary spermatocytes at early prophase or pachytene stage and Sertoli cells, the prepubertal group (including 3- and 4-week-old testes) further contained round, elongating, and elongated spermatids. In the pubertal, postpubertal, and aged

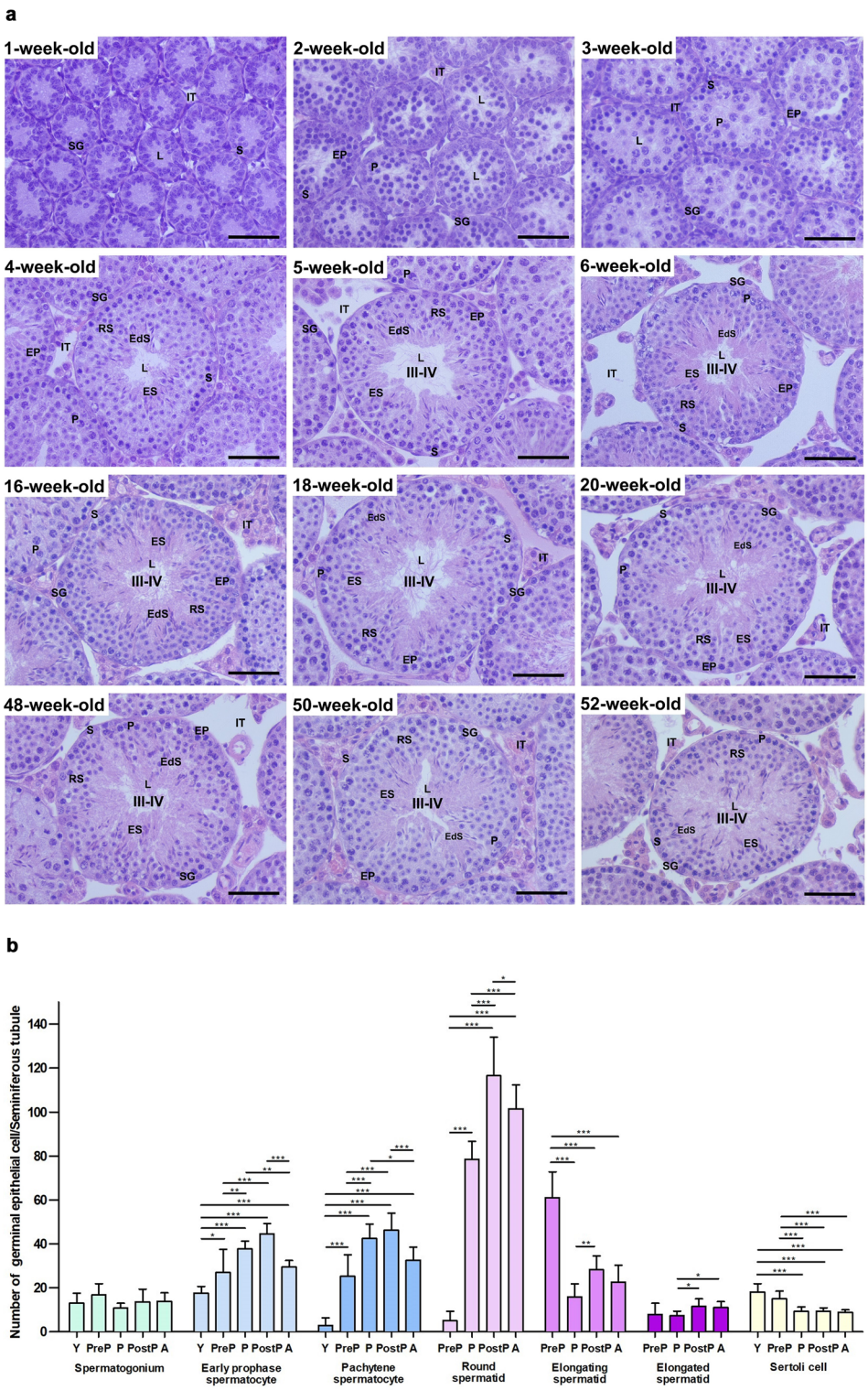

Fig. 1 **a** Representative micrographs of the postnatal mouse testes from 1 to 52 weeks of age. We evaluated histological structures of the hematoxylin and eosin (HE)-stained testis tissues, obtained from mice at the ages of 1, 2, 3, 4, 5, 6, 16, 18, 20, 48, 50, and 52 weeks. All the testes exhibited normal histological structures, and some differences related to having germ cell types were noted. The micrographs were captured at 400× original magnification. The scale bars represent 50 µm. **b** Numbers of the germinal epithelial cells in each group. We counted the germ cells from spermatogonia to elongated spermatids, and Sertoli cells per seminiferous tubule. Notably, randomly selected ten seminiferous tubules from at least four mice from each age were counted. We found that numbers of the primary spermatocytes at early prophase or pachytene stage, round spermatids, and Sertoli cells in the aged group were significantly lower compared with the pubertal or postpubertal group ($P < 0.05$). Herein, the data were evaluated using one-way ANOVA followed by Tukey's post hoc test for all the cell counts. $P < 0.05$ was considered statistically significant. Values are presented as mean ± standard error of the mean (SEM). *, $P < 0.05$; **, $P < 0.01$; ***, $P < 0.001$. *Y* young, *PreP* prepubertal, *P* pubertal, *PostP* postpubertal, *A* aged

groups, all germ cell types from spermatogonia to sperm cells as well as Sertoli cells were detected (Fig. 1a).

When we counted the germ cells from spermatogonia to elongated spermatids as well as Sertoli cells (Fig. 1b), no significant change was determined for spermatogonial cells among the groups. The early prophase and pachytene spermatocyte numbers progressively increased from young to postpubertal groups and sharply decreased in the aged group ($P < 0.05$). Round spermatids at the lowest number in the prepubertal group ($P < 0.001$) progressively increased

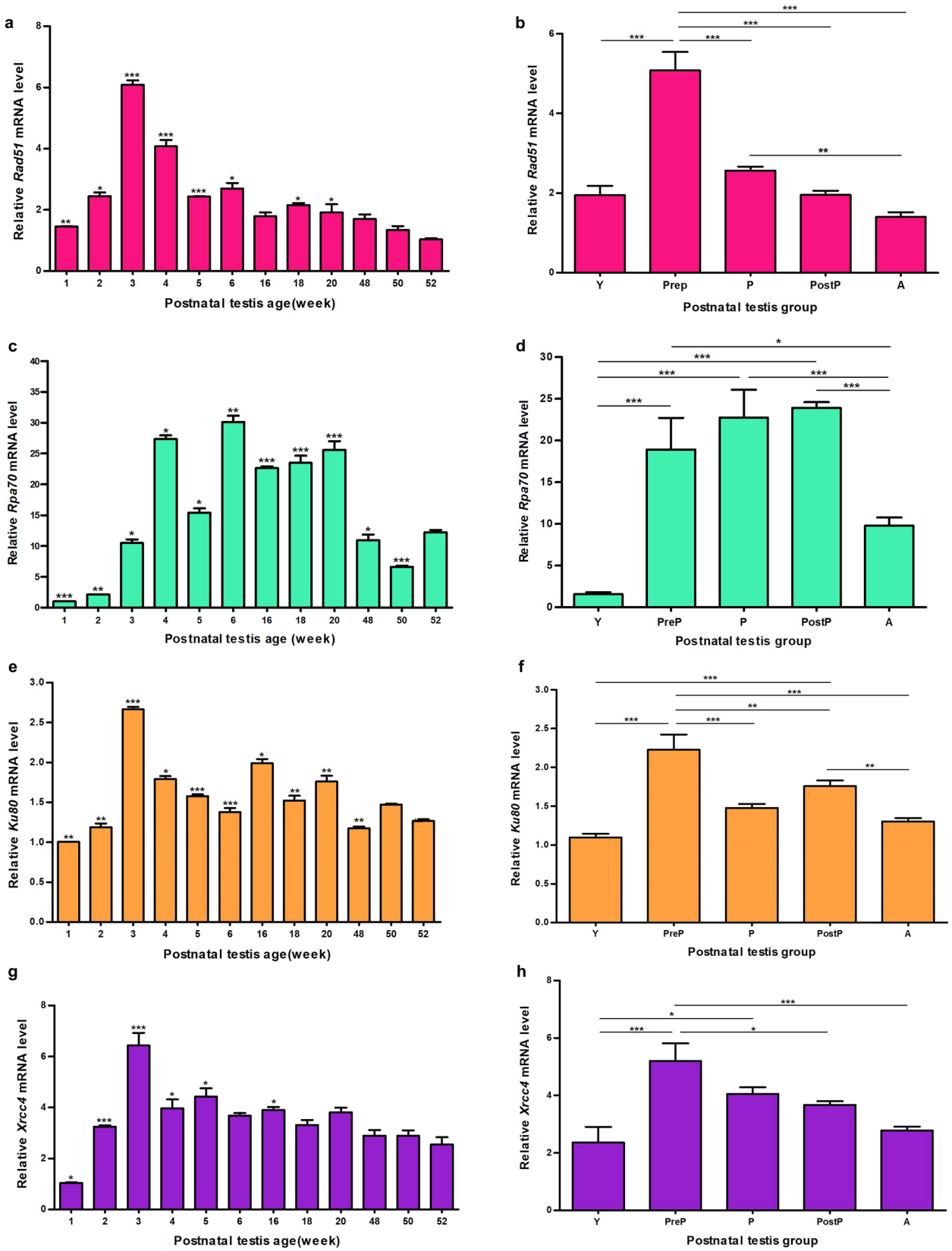
a
Relative Rad51 mRNA level
Postnatal testis age(week)
b
Relative Rad51 mRNA level
Y
Prep
P
PostP
A
Postnatal testis group
c
Relative Rpa70 mRNA level
Postnatal testis age (week)
d
Relative Rpa70 mRNA level
Y
PreP
P
PostP
A
Postnatal testis group
e
Relative Ku80 mRNA level
Postnatal testis age(week)
f
Relative Ku80 mRNA level
Y
PreP
P
PostP
A
Postnatal testis group
g
Relative Xrcc4 mRNA level
Postnatal testis age(week)
h
Relative Xrcc4 mRNA level
Y
PreP
P
PostP
A
Postnatal testis group

◂**Fig. 2** The relative expression of *Rad51*, *Rpa70*, *Ku80*, and *Xrcc4* genes in the postnatal mouse testes at different ages (at least four mice from each week), and in the young ($n=10$), prepubertal ($n=8$), pubertal ($n=8$), postpubertal ($n=12$), and aged ($n=17$) groups. We determined their expression levels using quantitative real-time polymerase chain reaction (qRT-PCR). Notably, *β-Actin* was used as a housekeeping gene for the normalization of target gene expression. **a** *Rad51* mRNA levels in the postnatal testes at different ages. The levels progressively increased from 1- to 3-week-old testes ($P<0.05$) and then gradually decreased toward 52-week-old testis ($P<0.05$). The *Rad51* gene expression in 52-week-old testis was set to 1. **b** *Rad51* mRNA levels among the groups, which exhibited the highest and lowest levels in the prepubertal and aged groups, respectively ($P<0.01$). The *Rad51* gene expression in the aged group was set to 1. **c** *Rpa70* mRNA levels in the postnatal testes at different ages. There were fluctuations in expression from 1- to 52-week-old testes ($P<0.05$). The *Rpa70* gene expression in 1-week-old testis was set to 1. **d** *Rpa70* mRNA levels among the groups. The aged group had lower levels compared with the prepubertal, pubertal, and postpubertal groups ($P<0.05$). The *Rpa70* gene expression in the young group was set to 1. **e** *Ku80* mRNA levels in the postnatal testes at different ages. We observed fluctuations in expression from 1- to 52-week-old testes ($P<0.05$). The *Ku80* gene expression in 1-week-old testis was set to 1. **f** *Ku80* mRNA levels among the groups. The aged group had a lower level in comparison with the other groups ($P<0.01$), except for the young one. The *Ku80* gene expression in the young group was set to 1. **g** *Xrcc4* mRNA levels in the postnatal testes at different ages. We found the lowest expression in 1-week-old ($P<0.05$) and highest level in 3-week-old testes ($P<0.01$). The *Xrcc4* gene expression in 1-week-old testis was set to 1. **h** *Xrcc4* mRNA levels among the groups. It was at the lowest level in the young group ($P<0.05$), significantly increased in the prepubertal group ($P<0.001$) and then gradually decreased toward aged group ($P<0.001$). The *Xrcc4* gene expression in the young group was set to 1. It is noteworthy that the data were evaluated using one-way ANOVA followed by Tukey's post hoc test for all genes. $P<0.05$ was considered statistically significant. We presented the values as mean ± standard deviation (SD). *, $P<0.05$; **, $P<0.01$; ***, $P<0.001$. *Y* young, *PreP* prepubertal, *P* pubertal, *PostP* postpubertal, *A* aged

toward postpubertal group ($P<0.001$), and decreased in the aged group ($P<0.05$). The prepubertal group had the highest elongating spermatid number ($P<0.001$), and the pubertal group possessed a lower number than that of the postpubertal group ($P<0.05$). When counting elongated spermatids, the aged and postpubertal groups had higher numbers compared with the pubertal group ($P<0.05$). On the other hand, the number of Sertoli cells gradually decreased from young to aged groups ($P<0.001$, Fig. 1b).

Rad51, *Rpa70*, *Ku80*, and *Xrcc4* gene expression in the postnatal testes

Herein, we determined the *Rad51*, *Rpa70*, *Ku80*, and *Xrcc4* mRNA levels in all weeks and groups from young to aged (Fig. 2). *Rad51* mRNA level progressively increased from 1- to 3-week-old testes ($P<0.05$) and gradually decreased to 5-week-old testis ($P<0.001$, Fig. 2a). After *Rad51* exhibited a fluctuated expression from 6- to 18-week-old testes ($P<0.05$), we observed gradual decreases toward 52-week-old testis ($P<0.05$, Fig. 2a). Among the groups (Fig. 2b), *Rad51* mRNA level significantly increased from young to prepubertal groups ($P<0.001$) and then gradually decreased toward the aged group ($P<0.01$). It is worth noting that the prepubertal and aged groups had the highest and lowest *Rad51* expression levels, respectively ($P<0.01$).

The *Rpa70* expression was at the lowest level in 1-week-old testis ($P<0.001$) and reached the highest level in 6-week-old testis ($P<0.01$, Fig. 2c). Sharply increased *Rpa70* expression in 4- and 6-week-old testes exhibited gradual increases from 1- to 20-week-old testes and then remarkably decreased in 48-, 50-, and 52-week-old testes ($P<0.05$, Fig. 2c). Among the groups (Fig. 2d), the lowest *Rpa70* expression in the young group progressively increased toward postpubertal group ($P<0.001$) and then dramatically reduced in the aged group ($P<0.05$).

The *Ku80* gene exhibited fluctuating expression patterns from 1- to 52-week-old testes ($P<0.05$, Fig. 2e). It was at the lowest and highest levels in 1- and 3-week-old testes, respectively ($P<0.01$). In the postnatal testis groups (Fig. 2f), *Ku80* expression at the lowest level in the young group ($P<0.001$) significantly increased in the prepubertal group ($P<0.001$), and then decreased in the pubertal group ($P<0.001$). The minimally enhanced *Ku80* mRNA level in the postpubertal group reduced again in the aged group ($P<0.01$, Fig. 2f). We think that fluctuations in the expression among groups may derive from different transcriptional activity of the *Ku80* gene in the testicular cells.

Expression of the other cNHEJ component, *Xrcc4*, was at the lowest level in 1-week-old testis ($P<0.01$) and increased progressively toward 3-week-old testis ($P<0.001$, Fig. 2g). Subsequently, there were fluctuations in the expression from 4- to 52-week-old testes ($P<0.05$). In the groups, we found *Xrcc4* expression at the lowest level in the young group ($P<0.05$), which dramatically increased in the prepubertal group ($P<0.001$) and then gradually decreased toward the aged group ($P<0.05$, Fig. 2h).

Expression of the γH2AX, RAD51, RPA70, KU80, and XRCC4 proteins in the postnatal testes

In the present study, we evaluated cellular distributions and relative levels of the γH2AX, RAD51, RPA70, KU80, and XRCC4 proteins in the postnatal testes from young to aged groups.

Cellular distribution and relative level of γH2AX

In all ages, we detected intense γH2AX immunoexpression in the spermatogonial cells and primary spermatocytes at early prophase stages, especially at preleptotene, and weak expression was noted in the pachytene spermatocytes. It is important to note that the XY bodies being formed by sex

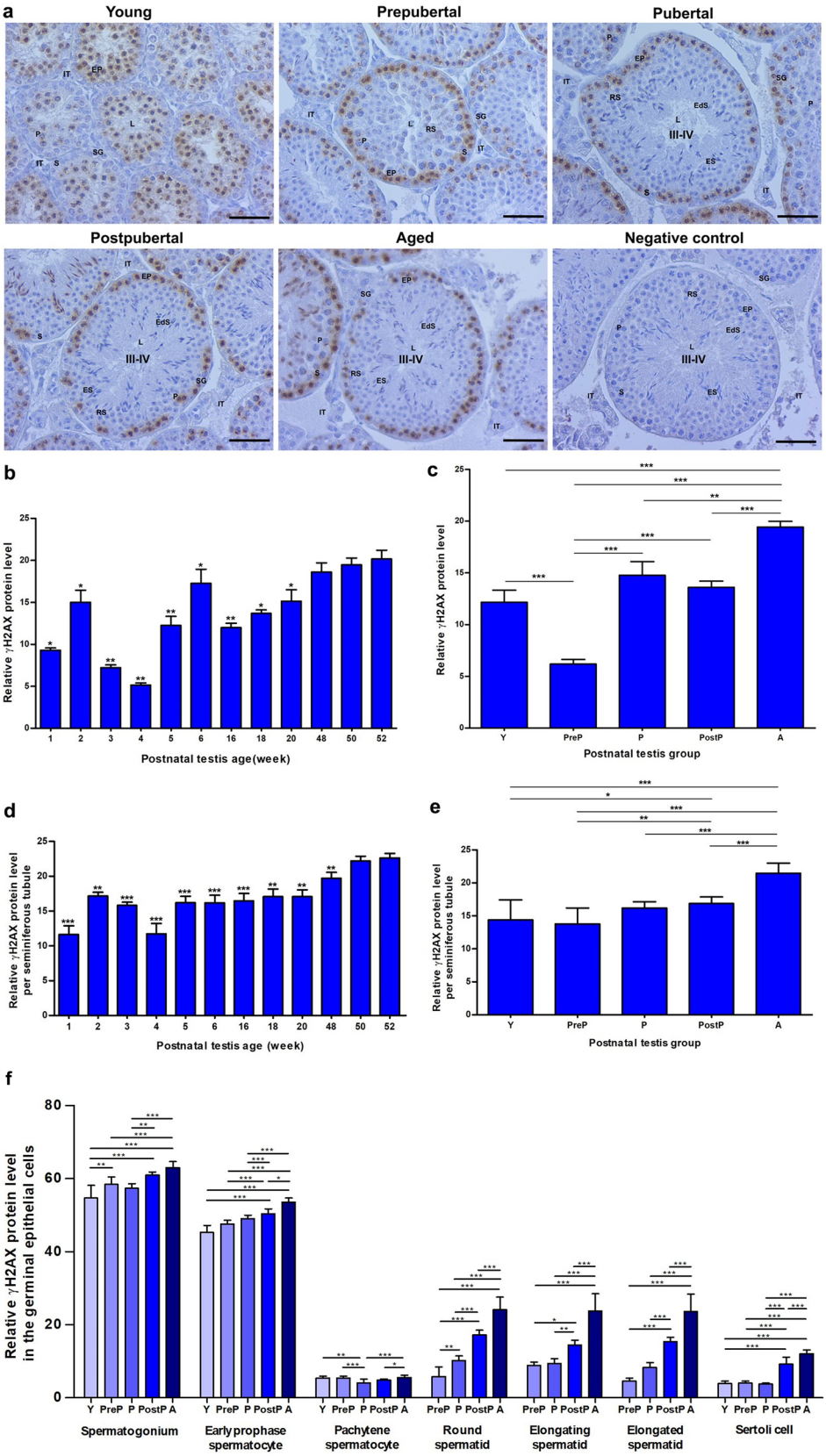
a
Young
Prepubertal
Pubertal
Postpubertal
Aged
Negative control
b
Relative γH2AX protein level
Postnatal testis age(week)
c
Relative γH2AX protein level
Y
PreP
P
PostP
A
Postnatal testis group
d
Relative γH2AX protein level per seminiferous tubule
Postnatal testis age (week)
e
Relative γH2AX protein level per seminiferous tubule
Postnatal testis group
f
Relative γH2AX protein level in the germinal epithelial cells
Spermatogonium
Early prophase spermatocyte
Pachytene spermatocyte
Round spermatid
Elongating spermatid
Elongated spermatid
Sertoli cell

◂**Fig. 3** The cellular distributions and relative levels of the γH2AX protein in the postnatal mouse testes. **a** Representative micrographs of γH2AX immunostaining in the young, prepubertal, pubertal, postpubertal, and aged groups. γH2AX exhibited strong nuclear localization in the spermatogonial cells and primary spermatocytes at the early prophase stage in each group, and there were weak nuclear and cytoplasmic intensities in the remaining germ cells and Sertoli cells. The micrographs were captured at 400× original magnification. Scale bars, 50 µm. **b** γH2AX levels in the testes at the different ages from 1 to 52 weeks. Generally, they increased toward the late ages, including 48-, 50-, and 52-week-old testes ($P < 0.05$). **c** γH2AX levels in the postnatal testis groups. They were at the highest level in the aged group compared with the other groups ($P < 0.01$). **d** γH2AX levels per seminiferous tubule in each age. They reached the highest levels in the late ages, that is, 48-, 50-, and 52-week-old testes ($P < 0.05$). **e** γH2AX levels per seminiferous tubule in each group. The aged group had a higher level than the other groups ($P < 0.05$). **f** γH2AX levels in the germinal epithelial cells of the postnatal testis groups. Despite some fluctuations in expression, they increased toward the aged group in spermatogonial cells, early prophase spermatocytes, round spermatids, elongating spermatids, elongated spermatids, and Sertoli cells ($P < 0.05$). The data were analyzed using one-way ANOVA followed by Tukey's post hoc test. $P < 0.05$ was considered statistically significant. We present the values as mean ± standard deviation (SD). *, $P < 0.05$; **, $P < 0.01$; ***, $P < 0.001$. *Y* young, *PreP* prepubertal, *P* pubertal, *PostP* postpubertal, *A* aged, *SG* spermatogonium, *EP* early prophase spermatocyte, *P* pachytene spermatocyte, *RS* round spermatid, *ES* elongating spermatid, *EdS* elongated spermatid, *S* Sertoli cell, *L* lumen, *IT* intertubular area

chromosomes were observed in the pachytene spermatocytes from 2-week-old testis onward. Additionally, the elongating and elongated spermatids from 3-week-old testis expressed γH2AX at a moderate intensity (Fig. 3a). Evaluating relative γH2AX levels in the testes at different ages (Fig. 3b) revealed a reduction from 1- to 4-week-old testes ($P < 0.05$), except for 2-week-old testis, which showed a sharp increase ($P < 0.05$). Subsequently, γH2AX levels progressively increased from 5- to 52-week-old testes ($P < 0.05$), except for 6-week-old testis, which exhibited a dramatic increase ($P < 0.05$). In the postnatal testis groups (Fig. 3c), γH2AX levels decreased from young to prepubertal groups ($P < 0.001$), remarkably enhanced in the pubertal/postpubertal groups ($P < 0.001$), and reached the highest level in the aged group ($P < 0.01$).

We also analyzed γH2AX levels in seminiferous tubules of the testes at different ages (Fig. 3d). They significantly increased from 1- to 2-week-old testes, decreased toward 4-week-old testis ($P < 0.01$), and progressively increased toward 52-week-old testis ($P < 0.01$). Among groups (Fig. 3e), although there were no significant changes between young, prepubertal, and pubertal groups, the postpubertal group had a higher level than the prepubertal ($P < 0.01$) and young ($P < 0.05$) groups. Importantly, the aged group exhibited the highest γH2AX level compared with the other groups ($P < 0.001$, Fig. 3e).

Evaluating γH2AX levels in the germinal epithelial cells (Fig. 3f), we found that they gradually increased from young to aged groups (except for the minimal decreases in several cell types of the pubertal group) in the spermatogonial cells ($P < 0.01$), early prophase spermatocytes ($P < 0.05$), round spermatids ($P < 0.01$), elongating spermatids ($P < 0.05$), elongated spermatids ($P < 0.001$), and Sertoli cells ($P < 0.001$). In the pachytene spermatocytes, γH2AX levels decreased from young/prepubertal groups to the pubertal group ($P < 0.01$), and then gradually increased toward the aged group ($P < 0.05$).

Cellular distribution and relative level of RAD51

We observed RAD51 immunoexpression in both intertubular area and seminiferous tubules in all ages (Fig. 4a). In the intertubular area, several cells, including Leydig cells and endothelial cells, exhibited immunostaining. In the seminiferous tubules, the germ cells from spermatogonia to elongated spermatids and Sertoli cells had nuclear and cytoplasmic RAD51 expression. Importantly, the primary spermatocytes at early prophase or pachytene stage possessed stronger RAD51 intensity in their nuclear region as compared with cytoplasm (Fig. 4a). When we analyzed relative RAD51 levels in the total area of each age (Fig. 4b), they gradually decreased from 1- to 16-week-old testes ($P < 0.05$) and then progressively increased from 18- to 48–52-week-old testes ($P < 0.05$). Among the groups (Fig. 4c), we detected the highest RAD51 level in the young group ($P < 0.001$), which significantly decreased toward the pubertal/postpubertal groups ($P < 0.05$). Subsequently, it increased again in the aged group ($P < 0.01$).

Evaluating RAD51 levels in the seminiferous tubules of each age (Fig. 4d) revealed an increase from 1- to 3-week-old testes and then decrease toward 52-week-old testis ($P < 0.05$), except for the minimal increase in 16-week-old testis ($P < 0.05$). In the groups (Fig. 4e), we found that RAD51 levels significantly increased from young to prepubertal groups ($P < 0.001$), and then gradually decreased toward aged group ($P < 0.05$).

When we measured the RAD51 levels in each germinal epithelial cell (Fig. 4f), no significant changes were discovered in the round, elongating, and elongated spermatids. In contrast, RAD51 levels in the spermatogonial cells reduced from young to postpubertal groups ($P < 0.001$) and remarkably increased in the aged group ($P < 0.001$). The early prophase and pachytene spermatocytes showed fluctuations in the expression from young to aged groups ($P < 0.05$). In the Sertoli cells, we noticed a gradual decrease for the RAD51 levels from young to aged groups ($P < 0.05$, Fig. 4f).

Cellular distribution and relative level of RPA70 protein

On analyzing expression distribution of another HR-repair component, RPA70 in the postnatal testes (Fig. 5a), we detected immunostaining either in the seminiferous tubules or

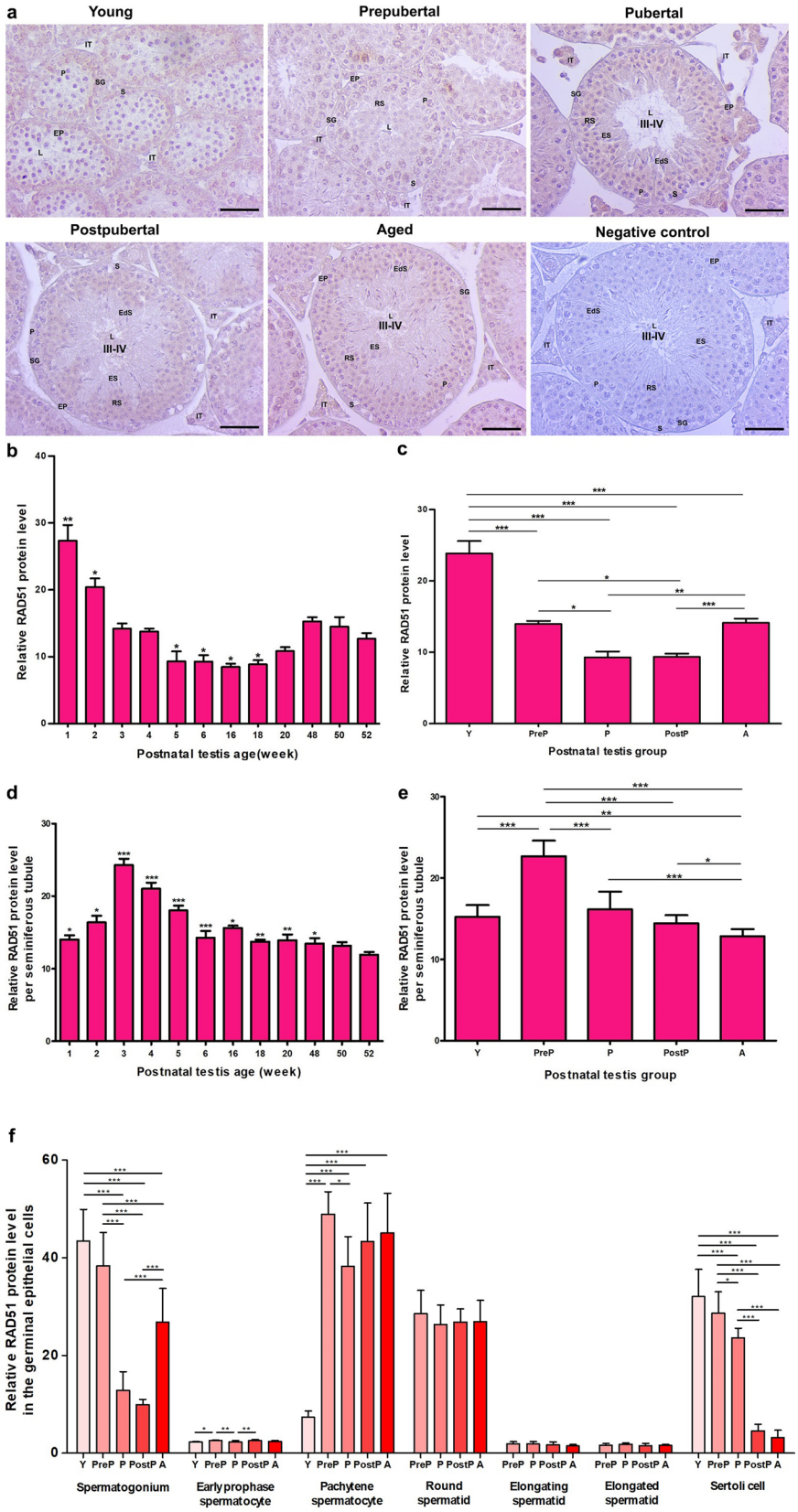
a
Young
Prepubertal
Pubertal
Postpubertal
Aged
Negative control
b
Relative RAD51 protein level
Postnatal testis age(week)
c
Relative RAD51 protein level
Y PreP P PostP A
Postnatal testis group
d
Relative RAD51 protein level per seminiferous tubule
Postnatal testis age (week)
e
Relative RAD51 protein level per seminiferous tubule
Y PreP P PostP A
Postnatal testis group
f
Relative RAD51 protein level in the germinal epithelial cells
Spermatogonium
Early prophase spermatocyte
Pachytene spermatocyte
Round spermatid
Elongating spermatid
Elongated spermatid
Sertoli cell

◂**Fig. 4** The cellular distributions and relative levels of the RAD51 protein in the postnatal mouse testes. **a** Representative micrographs of RAD51 immunostaining in the young, prepubertal, pubertal, postpubertal, and aged groups. RAD51 exhibited strong nuclear localization in the primary spermatocytes, and there were weak nuclear and cytoplasmic intensities in the remaining germ cells and Sertoli cells. The micrographs were captured at 400× original magnification. Scale bars, 50 µm. **b** RAD51 levels in the testes at the different ages from 1 to 52 weeks. They were gradually decreased from 1- to 16-week-old testes and then increased from 18 weeks to the late ages ($P<0.05$). **c** RAD51 levels in the postnatal testis groups. They significantly decreased from young to pubertal/postpubertal groups and subsequently increased in the aged group ($P<0.05$). **d** RAD51 levels per seminiferous tubule in each age. We detected that RAD51 levels progressively increased from 1- to 3-week-old testes ($P<0.05$) and then decreased toward 52-week-old testis ($P<0.05$). **e** RAD51 levels per seminiferous tubule in each group. The levels were low in the young group, significantly increased in the prepubertal group, and gradually decreased toward the aged group ($P<0.05$). **f** RAD51 levels in the germinal epithelial cells of the postnatal testis groups. We observed significant changes in the spermatogonial cells, early prophase spermatocytes, pachytene spermatocytes, and Sertoli cells among groups ($P<0.05$). The data were analyzed using one-way ANOVA followed by Tukey's post hoc test. $P<0.05$ was considered statistically significant. We present the values as mean ± standard deviation (SD). *, $P<0.05$; **, $P<0.01$; ***, $P<0.001$. *Y* young, *PreP* prepubertal, *P* pubertal, *PostP* postpubertal, *A* aged, *SG* spermatogonium, *EP* early prophase spermatocyte, *P* pachytene spermatocyte, *RS* round spermatid, *ES* elongating spermatid, *EdS* elongated spermatid, *S* Sertoli cell, *L* lumen, *IT* intertubular area

in the intertubular cells. There were weak nuclear and cytoplasmic RPA70 intensities in the intertubular cells, including Leydig cells and endothelial cells. In the seminiferous tubules, spermatogonial cells and pachytene spermatocytes exhibited strong expression in their nuclear and cytoplasmic regions. On the other hand, we determined weak nuclear and cytoplasmic immunoexpression in the other germinal epithelial cells, including early prophase spermatocytes, round, elongating, and elongated spermatids, and Sertoli cells. Total RPA70 levels in the testes at different ages (Fig. 5b) progressively reduced from 1- to 4-week-old testes ($P<0.05$) and then increased toward 6-week-old testis ($P<0.05$). Subsequently, the RPA70 levels decreased from 6- to 20-week-old testes ($P<0.05$) and increased again at the late ages, including 48-, 50-, and 52-week-old testes. In the postnatal testis groups (Fig. 5c), no significant differences were found between prepubertal, pubertal, and postpubertal groups; the young group had a higher level compared with the prepubertal, pubertal, and postpubertal groups ($P<0.05$). Also, the aged group possessed a higher RPA70 level than the prepubertal and postpubertal groups ($P<0.001$).

The RPA70 levels per seminiferous tubule (Fig. 5d) progressively increased from 1- to 20-week-old testes ($P<0.05$), and then decreased toward 52-week-old testis ($P<0.001$). Among groups (Fig. 5e), RPA70 levels increased from young to postpubertal groups ($P<0.01$) and then reduced in the aged group ($P<0.001$).

When we evaluated RPA70 levels in the germinal epithelial cells, there were cell-type-specific differences among groups (Fig. 5f). In the spermatogonial cells, the young group had a higher level than the pubertal group ($P<0.05$). The early prophase spermatocytes of the young group exhibited the highest level in comparison with the other groups ($P<0.001$). For the same cell type, the prepubertal and aged groups possessed higher levels than the pubertal group ($P<0.01$), and similarly, the aged group had higher expression than the postpubertal group ($P<0.05$). In the pachytene spermatocytes, RPA70 had the lowest level in the young group ($P<0.001$), increased in the prepubertal group ($P<0.01$), and further increased in the pubertal, postpubertal, and aged groups ($P<0.05$). The round spermatids of the prepubertal group exhibited lower RPA70 level than the pubertal and postpubertal groups ($P<0.001$) and had lower expression in the aged group than in the postpubertal group ($P<0.05$). We observed the same expression distribution in the elongating and elongated spermatids, in which RPA70 levels progressively increased from prepubertal to aged groups ($P<0.05$). In the Sertoli cells, it increased from young to postpubertal/aged groups ($P<0.01$).

Cellular distribution and relative level of KU80

A cNHEJ component KU80 was expressed in the intertubular area and seminiferous tubules of all testes from 1 to 52 weeks of age (Fig. 6a). There was cytoplasmic and nuclear immunoexpression in the Leydig cells and endothelial cells, localized in the intertubular area. In the seminiferous tubules, we detected strong KU80 intensity in the nuclear region of pachytene spermatocytes. The weak nuclear and cytoplasmic immunoexpression were observed in the spermatogonial cells, round spermatids, and Sertoli cells. It is noteworthy that there was a very weak KU80 intensity in the preleptotene spermatocytes and elongating and elongated spermatids (Fig. 6a). Relative KU80 levels in the total area of the testes at different ages (Fig. 6b) had the lowest levels in 1- and 2-week-old testes compared with the other ages ($P<0.001$). Notably, no significant change was noted in the testes from 3 to 50 weeks of age. In the groups, we detected the lowest KU80 level in the young group in comparison with the other groups ($P<0.001$), and no significant changes were discovered among the other groups (Fig. 6c).

The seminiferous tubules of 1- and 2-week-old testes possessed significantly lower KU80 levels than those of the other ages ($P<0.001$, Fig. 6d). Importantly, KU80 levels remarkably decreased at the late ages, including 48-, 50-, and 52-week-old testes as compared with 3- to 20-week-old testes ($P<0.05$). In the postnatal groups, KU80 at the lowest level in the young group significantly increased in the prepubertal, pubertal, and postpubertal groups ($P<0.001$) and decreased in the aged

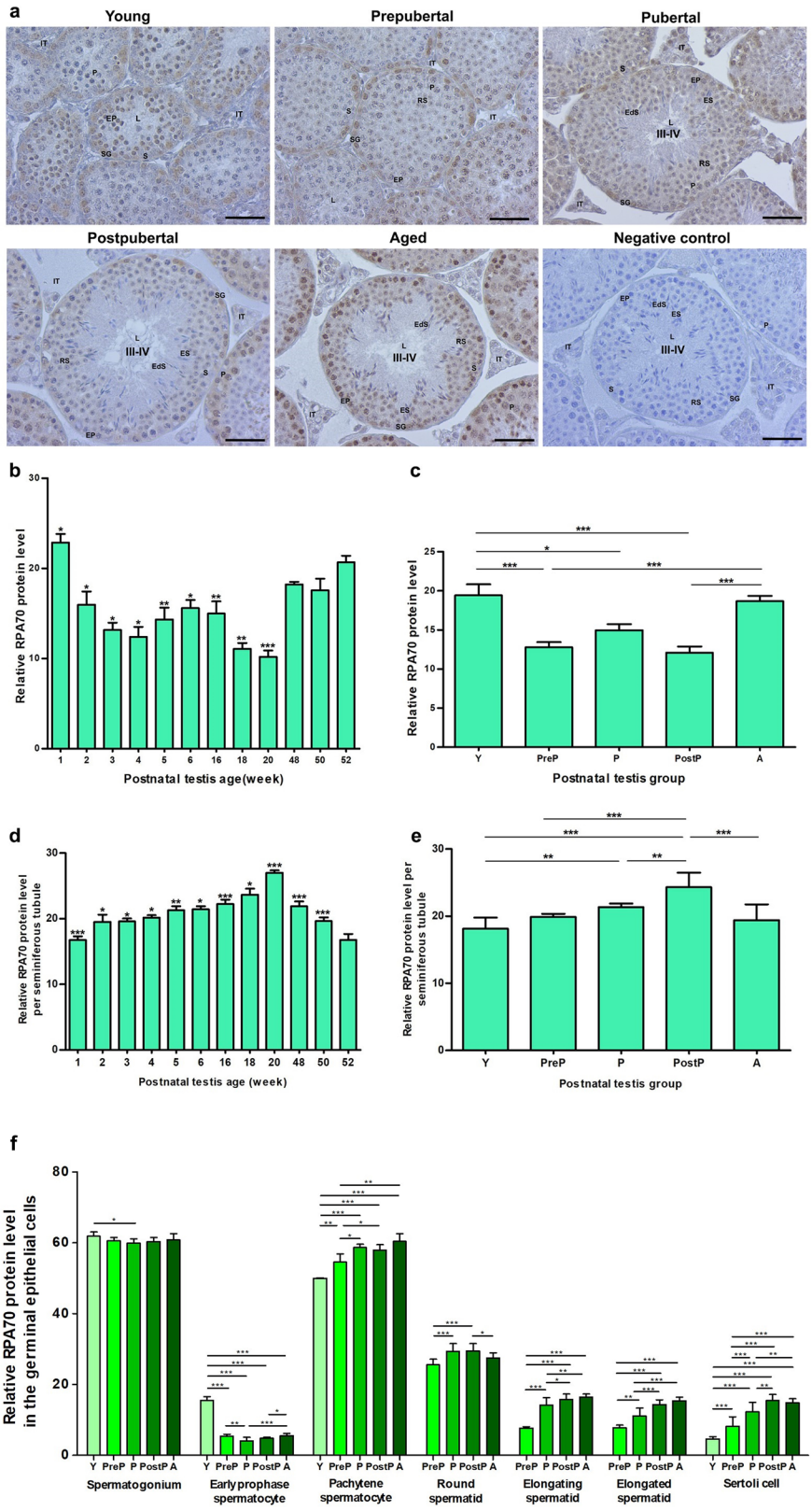

Fig. 5 The cellular distributions and relative levels of the RPA70 protein in the postnatal mouse testes. **a** Representative micrographs of RPA70 immunostaining in the young, prepubertal, pubertal, postpubertal, and aged groups. RPA70 exhibited strong nuclear localization in the spermatogonial cells and primary spermatocytes at pachytene stage, and there were weak nuclear and cytoplasmic intensities in the remaining germ cells and Sertoli cells. The micrographs were captured at 400× original magnification. Scale bars, 50 µm. **b** RPA70 levels in the testes at the different ages from 1 to 52 weeks. They showed fluctuations from 1- to 52-week-old testes ($P < 0.05$). **c** RPA70 levels in the postnatal testis groups. The levels were highest in the young and aged groups ($P < 0.05$). **d** RPA70 levels per seminiferous tubule in each age. We found that RPA70 level progressively increased from 1- to 20-week-old testes and then gradually decreased toward 52-week-old testis ($P < 0.05$). **e** RPA70 levels per seminiferous tubule in each group. They increased from young to postpubertal groups and reduced in the aged group ($P < 0.01$). **f** RPA70 levels in the germinal epithelial cells of the postnatal testis groups. We observed significant changes in all the cell types among groups ($P < 0.05$). The data were analyzed using one-way ANOVA followed by Tukey's post hoc test. $P < 0.05$ was considered statistically significant. We present the values as mean ± standard deviation (SD). *, $P < 0.05$; **, $P < 0.01$; ***, $P < 0.001$. *Y* young, *PreP* prepubertal, *P* pubertal, *PostP* postpubertal, *A* aged, *SG* spermatogonium, *EP* early prophase spermatocyte, *P* pachytene spermatocyte, *RS* round spermatid, *ES* elongating spermatid, *EdS* elongated spermatid, *S* Sertoli cell, *L* lumen, *IT* Intertubular area

group ($P < 0.001$). However, no difference was noted between prepubertal, pubertal, and postpubertal groups (Fig. 6e).

Upon analyzing KU80 levels in the germinal epithelial cells between groups (Fig. 6f), although we did not find any remarkable changes in the round, elongating, and elongated spermatids as well as Sertoli cells, the spermatogonial cells of the young group had the lowest KU80 level compared with the remaining groups ($P < 0.05$). In the early prophase spermatocytes, the young group possessed a lower level than the postpubertal group ($P < 0.05$). The pachytene spermatocytes of the young group had the lowest KU80 level ($P < 0.001$), but no further differences were determined among other groups.

Cellular distribution and relative level of XRCC4

In the seminiferous tubules (Fig. 7a), XRCC4 was intensively localized in the nuclear region of pachytene spermatocytes and round spermatids, and there was very weak immunoexpression in the spermatogonial cells, early prophase spermatocytes, elongating spermatids, elongated spermatids, and Sertoli cells. It is worth noting that XRCC4 immunoreactivity was at a low intensity in the intertubular cells, including Leydig cells and endothelial cells (Fig. 7a). Relative XRCC4 levels in the testes at different ages (Fig. 7b) progressively increased from 1- to 20-week-old testes ($P < 0.05$) and then minimally decreased in 48-, 50-, and 52-week-old testes. In the postnatal testis groups (Fig. 7c), XRCC4 levels progressively enhanced from young to aged groups ($P < 0.01$).

The XRCC4 levels per seminiferous tubule (Fig. 7d) increased from 1- to 18-/20-week-old testes ($P < 0.05$) and remained at high levels in 48-, 50-, and 52-week-old testes ($P < 0.05$). Among groups (Fig. 7e), we found that XRCC4 levels increased from young to postpubertal/aged groups ($P < 0.01$). In the germinal epithelial cells of the groups, no significant changes existed in the spermatogonial cells, elongating spermatids, elongated spermatids, and Sertoli cells (Fig. 7f). The early prophase spermatocytes of the aged group had lower XRCC4 levels than the prepubertal and pubertal groups ($P < 0.05$), and the prepubertal group had higher expression than the postpubertal group ($P < 0.01$). In the pachytene spermatocytes, the young group possessed the lowest level in comparison with the other groups ($P < 0.001$). The round spermatids of the aged group expressed XRCC4 at a lower level compared with the prepubertal and pubertal groups ($P < 0.05$).

Discussion

In the current study, the *Rad51*, *Rpa70*, *Ku80*, and *Xrcc4* gene expression at mRNA and protein levels, as well as γH2AX profiles, were for the first time evaluated in the postnatal mouse testes from early to aged periods. We found that *Rad51*, *Rpa70*, *Ku80*, and *Xrcc4* mRNA levels significantly decreased in the aged group compared with the pubertal and postpubertal groups. The most likely reason for these decreases is the reduced numbers of primary spermatocytes at early prophase or pachytene stage, round spermatids, and Sertoli cells in the aged group. Immunostaining results of their encoded proteins revealed that they express these genes. It is noteworthy that reduced numbers of other testicular cells, such as Leydig cells, may also have contributed to the decreased mRNA levels. In parallel with our cell count results, previous studies reported that numbers of all germ cell types as well as testosterone production and spermatogenic activity, sperm production and quality predominantly declined during aging in men (Paniagua et al. 1991; Wolf et al. 2000; Tenover 2003; Santiago et al. 2019). Despite controversial results, Leydig cell (Neaves et al. 1984, 1985) and Sertoli cell (Johnson et al. 1984) counts were further found to decrease along with testicular aging.

Although we could not analyze gene expression in each cell type through cell isolation, reduced transcriptional activity in aged testicular cells may be another factor that led to decreased mRNA levels. Consistent with this prediction, Paul et al. (2013) revealed that transcriptional activity of the genes involved in the DNA repair processes, including DSB repair, base excision repair (BER), and nucleotide excision repair (NER), widely declines in the testicular cells undergoing biological aging (Paul et al. 2013). Serum testosterone levels decrease during aging (Bhasin et al. 2000; Snyder 2001), resulting in reduced transcriptional activation through the classical pathway by binding to androgen receptors or the noncanonical pathway (Fix et al. 2004; Walker 2010). Thus, a decrease in testosterone levels in the aged group may have reduced transcript levels of these genes.

Herein, we found *Rad51*, *Rpa70*, *Ku80*, and *Xrcc4* gene expression at lowest levels in the young group. Low numbers of the primary spermatocytes at early prophase or pachytene stage, round spermatids, and elongated spermatids, which transcribe these genes according to the immunostaining findings, may be a cause of decreased mRNA levels. Another reason might be a decrease in reproductive hormone levels, such as testosterone, in this period of life. It was evidenced in previous studies that testosterone was at lower levels in young mice compared with adult ones (Jean-Faucher et al. 1978; Anderson Jr et al. 1989). Since testosterone enables increase of transcriptional activity (Parada-Bustamante et al. 2017), its decreased level in the young group might underlie reduced gene expression.

γH2AX is a commonly used biomarker for defining DSBs arising from cytotoxic chemical agents as well as environmental and physical factors (Turinetto and Giachino 2015). Following phosphorylation of serine 139 by ataxia telangiectasia mutated (ATM) and ATM-Rad3-related (ATR) kinases

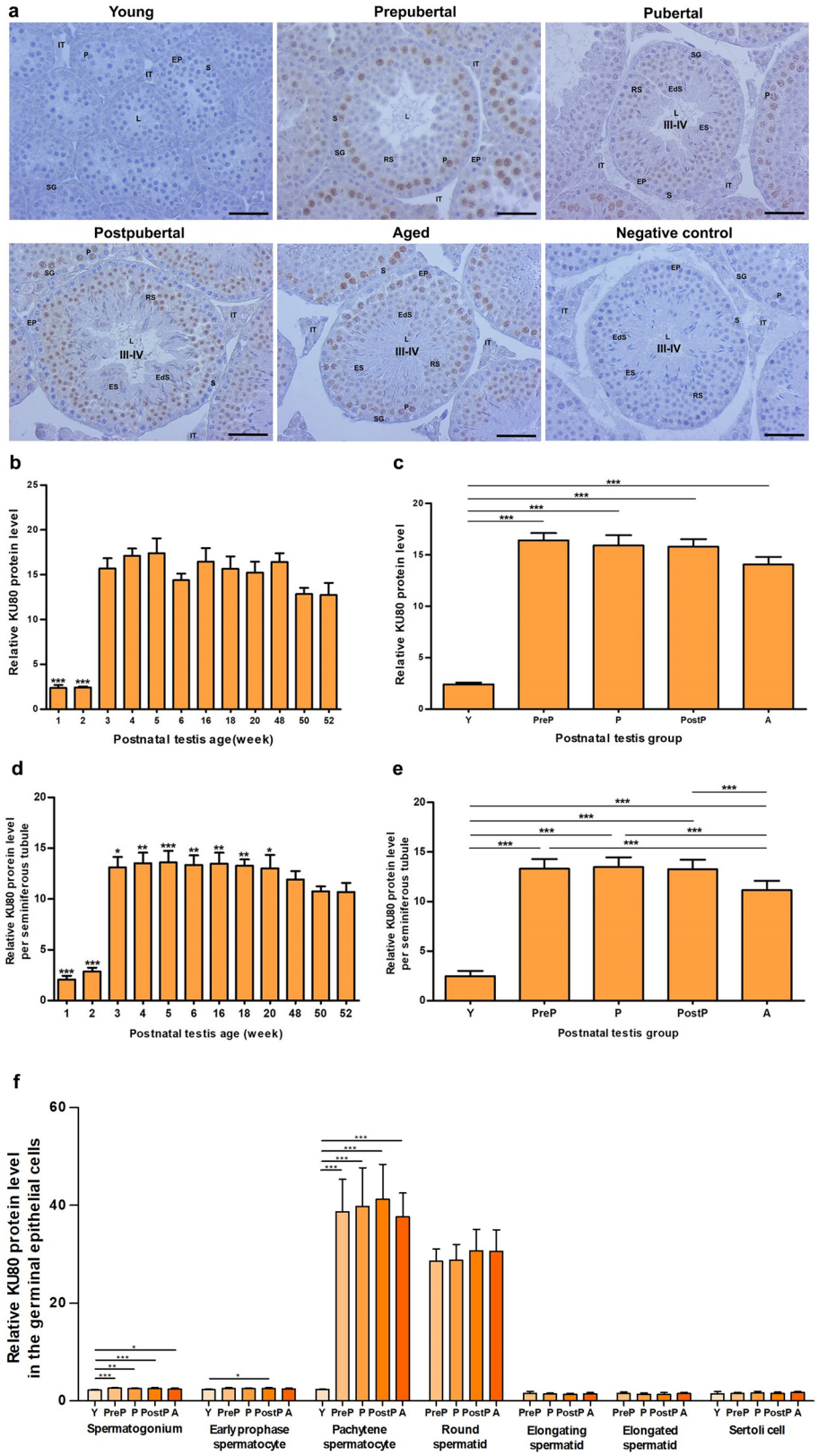
a
Young
Prepubertal
Pubertal
Postpubertal
Aged
Negative control
b
Relative KU80 protein level
Postnatal testis age(week)
c
Relative KU80 protein level
Postnatal testis group
Y
PreP
P
PostP
A
d
Relative KU80 prorein level per seminiferous tubule
Postnatal testis age (week)
e
Relative KU80 protein level per seminiferous tubule
Postnatal testis group
f
Relative KU80 protein level in the germinal epithelial cells
Spermatogonium
Early prophase spermatocyte
Pachytene spermatocyte
Round spermatid
Elongating spermatid
Elongated spermatid
Sertoli cell

◂**Fig. 6** The cellular distributions and relative levels of the KU80 protein in the postnatal mouse testes. **a** Representative micrographs of KU80 immunostaining in the young, prepubertal, pubertal, postpubertal, and aged groups. KU80 exhibited strong nuclear localization in the primary spermatocytes at pachytene stage, and weak nuclear and cytoplasmic intensities were noted in the remaining germ cells and Sertoli cells. The micrographs were captured at 400× original magnification. Scale bars, 50 µm. **b** KU80 levels in the testes at the different ages from 1 to 52 weeks of age. The levels were at lowest in 1- and 2-week-old testes ($P < 0.001$). **c** KU80 levels in the postnatal testis groups. The level was the lowest in the young group compared with the other groups ($P < 0.001$). **d** KU80 levels per seminiferous tubule in each age. KU80 was at lowest level in 1- and 2-week-old testes ($P < 0.001$), and 48-, 50-, and 52-week-old testes had lower levels than 3- to 20-week-old testes ($P < 0.05$). **e** KU80 levels per seminiferous tubule in each group. The young and aged groups possessed lower levels than the prepubertal, pubertal, and postpubertal groups ($P < 0.001$). **f** KU80 levels in the germinal epithelial cells of the postnatal testis groups. We observed significant decreases in the spermatogonial cells, early prophase spermatocytes, and pachytene spermatocytes of the young group ($P < 0.05$). The data were analyzed using one-way ANOVA followed by Tukey's post hoc test. $P < 0.05$ was considered statistically significant. We present the values as mean ± standard deviation (SD). *, $P < 0.05$; **, $P < 0.01$; ***, $P < 0.001$. *Y* young, *PreP* prepubertal, *P* pubertal, *PostP* postpubertal, *A* aged, *SG* spermatogonium, *EP* early prophase spermatocyte, *P* pachytene spermatocyte, *RS* round spermatid, *ES* elongating spermatid, *EdS* elongated spermatid, *S* Sertoli cell, *L* lumen, *IT* intertubular area

through PI3K (phosphoinositide 3-kinase) pathway, γH2AX recruits DSB repair proteins to damaged sites (Kuo and Yang 2008). Consistent with its basic functional features, we found γH2AX at highest levels in the spermatogonial cells and early prophase spermatocytes in the postnatal testes, as demonstrated in previous studies (Hamer et al. 2003; Forand et al. 2004). Many consecutive mitotic divisions necessitating rounds of DNA replication at the beginning of spermatogenesis in the spermatogonial cells (Griswold 2016) may lead to increase of DSBs. Additionally, exposing low-dose ionizing radiation results in the accumulation of DSBs in the spermatogonial cells (Grewenig et al. 2015). These DSBs can be repaired in the subsequent germline cells during spermatogenic progression. For proper crossing-over, a number of DSBs are created by the topoisomerase SPO11 at the early prophase stages (Lam and Keeney 2014). Therefore, DSB reaches high levels in the primary spermatocytes at early stages (Qu et al. 2021), as observed in the current study.

The aged group exhibited the highest γH2AX level as compared with the other groups. This increase likely originated from elevated γH2AX levels in all germinal epithelial cells from spermatogonia to Sertoli cells. Consistently, previous studies revealed that DSB levels increase in the sperm cells obtained from aged men (Singh et al. 2003; Paul and Robaire 2013; Muratori et al. 2019). The possible factors leading to increased DSBs in the germ cells during aging can be the elevated reactive oxygen species (ROS) levels (Cui et al. 2012), mitochondrial dysfunction (Cui et al. 2012), and decreased DSB repair efficiency (Gorbunova and Seluanov 2016).

In male germ cells, there are three main pathways, HR, cNHEJ, and aEJ, for repairing DSBs during spermatogenesis (Gunes et al. 2015). The major components of HR repair are the RAD51 and RPA70 proteins (Whelan et al. 2018). RAD51 accumulates at DSB sites to catalyze the exchange between damaged strand and sister strand to facilitate DSB repair (Baumann and West 1998; Robert et al. 2021). RAD51 immunoexpression was determined in the nuclear and cytoplasmic regions of mouse spermatocytes (Kuramochi-Miyagawa et al. 2004; Chen et al. 2016). In addition to pachytene spermatocytes, we detected RAD51 expression in both nuclear and cytoplasmic regions of spermatogonial cells and round spermatids in the postnatal testes. High expression of *Rad51* in these cells may be related to repairing preformed DSBs in the spermatogonial cells and early prophase spermatocytes. On the other hand, enhanced RAD51 level in the round spermatids suggests that it may contribute to repairing DSBs, which emerge in the transition process from histones to protamines, at the later periods of spermiogenesis.

Consistent with the high RAD51 level observed in the pachytene spermatocytes, Kamel et al. (1997) detected highest *Rad51* mRNA level in the late pachytene spermatocytes compared with the primary spermatocytes at different stages, spermatogonia, round spermatids, and Sertoli cells (Kamel et al. 1997). Increased RAD51 level in pachytene spermatocytes seems to be essential for maintaining their viability because its loss led to depletion of the primary spermatocytes at late prophase stage through apoptosis (Dai et al. 2017). The same researchers also observed that RAD51 localizes specifically in spermatogonial cells and primary spermatocytes from preleptotene to pachytene stages in mouse testes. These immunostaining patterns were largely similar to our results, in which only difference was the detection of weak immunoexpression in early prophase spermatocytes. In the seminiferous tubules of the aged group, RAD51 level significantly decreased compared with the pubertal and postpubertal groups. Reduced numbers of primary spermatocytes at early prophase and pachytene stages (highly expressed *Rad51*) and Sertoli cells may be one of the factors leading to this decrease. Another factor might be the decreased RAD51 translation in the early prophase spermatocytes and Sertoli cells.

A recent study by Nguyen-Powanda and Robaire demonstrated that biological aging did not change RAD51 level in mouse spermatocytes (Nguyen-Powanda and Robaire 2021). However, there was a significant decrease of RAD51 immunostaining in the spermatids at the seminiferous tubule stages of I–IV and VIII–IX in the aged mice (15–18 months) as compared with the young mice (3–4 months). Also,

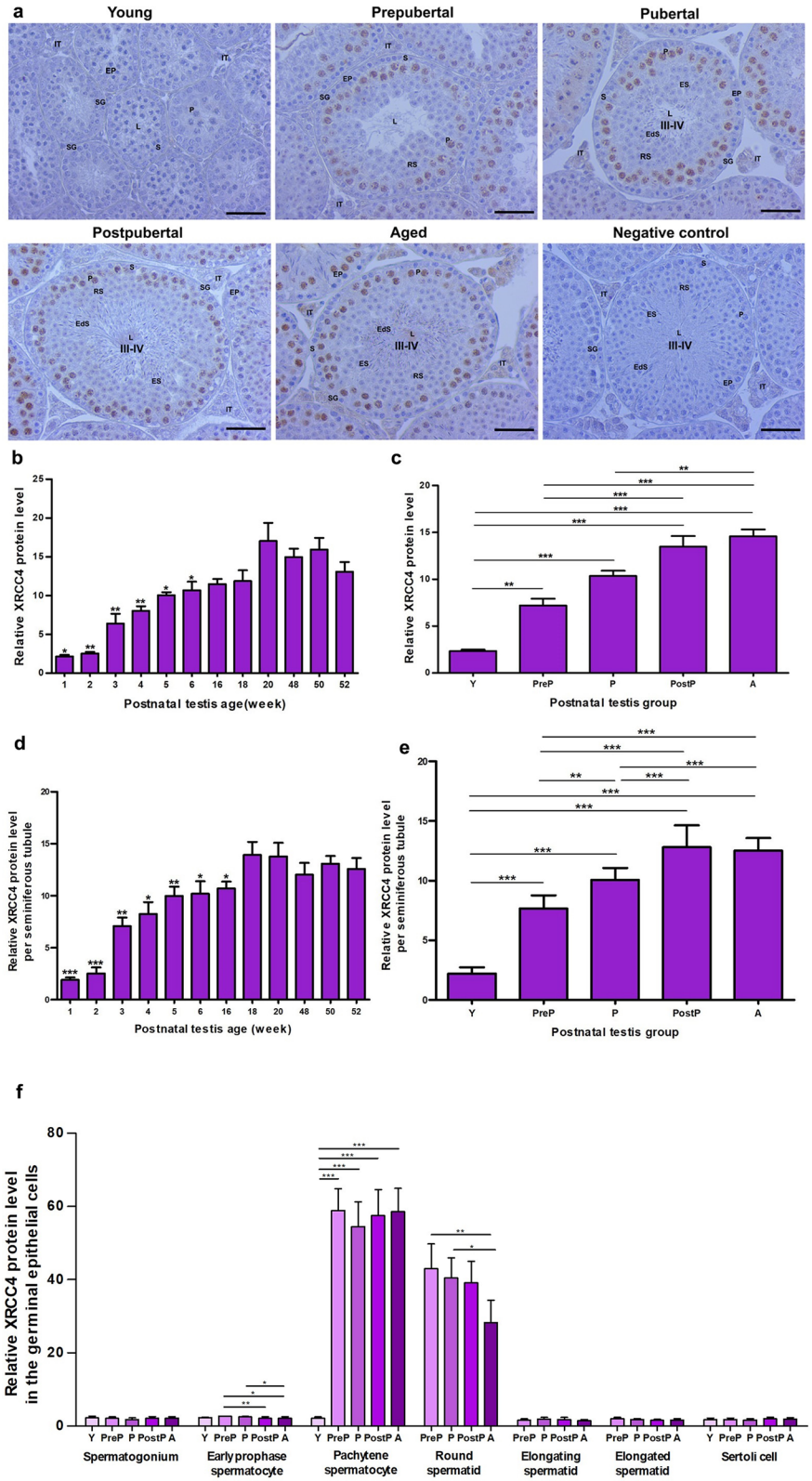

Rad51 expression predominantly decreased in the round spermatids of the aged mice. Similarly, we did not discover significant changes in the primary spermatocytes at early prophase and pachytene stages between postpubertal (named as young in this study) and aged groups. By contrast, no remarkable change in the spermatids was found among

◂**Fig. 7** The cellular distributions and relative levels of the XRCC4 protein in the postnatal mouse testes. **a** Representative micrographs of XRCC4 immunostaining in the young, prepubertal, pubertal, postpubertal, and aged groups. XRCC4 exhibited strong nuclear localization in the primary spermatocytes at pachytene stage and round spermatids, and there were weak nuclear and cytoplasmic intensities in the remaining germ cells and Sertoli cells. The micrographs were captured at 400× original magnification. Scale bars, 50 µm. **b** XRCC4 levels in the testes at the different ages from 1 to 52 weeks. They were gradually enhanced from 1- to 20-week-old testes and remained at high levels in 48-, 50-, and 52-week-old testes ($P < 0.05$). **c** XRCC4 levels in the postnatal testis groups. The XRCC4 level progressively increased from young to aged groups ($P < 0.01$). **d** XRCC4 levels per seminiferous tubule in each age. We detected highest levels in 18- to 52-week-old testes ($P < 0.05$). **e** XRCC4 levels per seminiferous tubule in each group. They gradually increased from young to postpubertal/aged groups ($P < 0.01$). **f** XRCC4 levels in the germinal epithelial cells of the postnatal testis groups. We observed significant changes in the primary spermatocytes at early prophase or pachytene stage and round spermatids among groups ($P < 0.05$). The data were analyzed using one-way ANOVA followed by Tukey's post hoc test. $P < 0.05$ was considered statistically significant. We present the values as mean ± standard deviation (SD). *, $P < 0.05$; **, $P < 0.01$; ***, $P < 0.001$. *Y* young, *PreP* prepubertal, *P* pubertal, *PostP* postpubertal, *A* aged, *SG* spermatogonium, *EP* early prophase spermatocyte, *P* pachytene spermatocyte, *RS* round spermatid, *ES* elongating spermatid, *EdS* elongated spermatid, *S* Sertoli cell, *L* lumen, *IT* intertubular area

these two groups in our study. This difference may derive from analyzing distinct seminiferous tubule stages and/or using different techniques for immunostaining.

Another key HR repair component RPA70 specifically binds to ssDNA to form a heterotrimeric structure so that the extended 3′-end site is covered (Yates et al. 2018; Marini et al. 2019). Additionally, RPA70 also plays roles in various cellular processes such as DNA replication and recombination, cell cycle control, and DNA damage checkpoints (Zou et al. 2006; Hinch et al. 2020). Expectedly, RPA70 deficiency in adult mouse testes caused uncovered extended single-strand ends of double helix and cessation of meiotic recombination at the zygotene stage of spermatocytes (Shi et al. 2019). Consequently, the rate of crossing-over was dramatically decreased in the primary spermatocytes.

In the present study, we found that RPA70 exhibited higher immunoexpression in the spermatogonial cells and pachytene spermatocytes of the postnatal groups. As RAD51 and RPA70 work together in the HR-based repair of DSBs appearing in spermatogonial cells and primary spermatocytes, they showed similar expression patterns in these germ cells during spermatogenesis. Decreased RPA70 expression in the seminiferous tubules of the aged group may result from its reduced level in the round spermatids as well as from declined numbers of the primary spermatocytes at early prophase or pachytene stage, round spermatids, elongating spermatids, and Sertoli cells. On the other hand, RPA70 levels in the germinal epithelial cells, except for spermatogonial cells and round spermatids, reached high levels in the aged group. These increases might occur to repair elevated DSBs in the aged germinal epithelial cells. To the best of our knowledge, no study has examined the molecular background of changed *Rpa70* expression in aged testicular cells. Thus, further studies are required to reveal the mechanisms and factors regulating RPA70 levels in aged germinal epithelial cells as well as intertubular cells.

The KU proteins, KU70 and KU80, contribute to repairing DSBs through cNHEJ pathway (Fell and Schild-Poulter 2015). Their immunoexpression was detected in mouse spermatogonial cells, primary spermatocytes at late pachytene or diplotene stage, and Sertoli cells (Ahmed et al. 2007). Likewise, we observed higher KU80 immunoreactivity in the pachytene spermatocytes and round spermatids compared with the other cells. Since DSBs are formed in the early spermatocytes before crossing-over, KU80 levels increased in the primary spermatocytes at pachytene stage and round spermatids to promote their repair. Low KU80 expression in the germinal epithelial cells, such as spermatogonia, early prophase spermatocytes, and elongating spermatids, suggests that cNHEJ repair activity may occur at minimal levels.

The aged and young groups had the lowest KU80 levels, most likely arising from decreased numbers of pachytene spermatocytes and round spermatids in these groups. In parallel with our study, an investigation on the rat testes at different ages (6, 12, 18, and 24 months) reported that KU80 levels significantly reduced in 18- and 24-month-old testes compared with the early periods (Um et al. 2003). As KU80 deficiency resulted in an increase in the spaces between broken DNA ends (Soutoglou et al. 2007), premature cellular senescence, and growth retardation in mice (Gu et al. 1997; Ouyang et al. 1997), the decreased KU80 levels in the aged testicular cells can lead to attenuation of cNHEJ repair efficiency that may cause emergence of age-related phenotypes, including fertility loss.

cNHEJ-related XRCC4 protein was also evaluated in the postnatal testes from young to aged groups. Like KU80, we found higher XRCC4 immunoexpression in the pachytene spermatocytes and round spermatids. As spermatogonial cells and pachytene spermatocytes contain DSBs, which was shown by γH2AX immunostaining, the XRCC4 levels reached high levels in those cells to repair preformed DSBs. Expression of the cNHEJ components, KU80 and XRCC4, in the germinal epithelial cells from spermatogonia to Sertoli cells at different levels indicates that cNHEJ seems to be worked in these cells, but possibly at distinct speed. We also demonstrated herein that XRCC4 levels progressively increased from young to postpubertal/aged groups. Since the aged and postpubertal groups had higher numbers of pachytene spermatocytes and round spermatids, XRCC4 could reach high levels in these groups.

XRCC4 is well known to undergo phosphorylation at its C-terminus by cyclin-dependent kinase 1 (CDK1) or polo-like kinase 1 (PLK1). Importantly, this posttranslational modification leads to suppression of its DSB repair activity (Terasawa et al. 2014). Therefore, it seems to be an important point to determine phosphorylated XRCC4 levels in the germinal epithelial cells of aged mice. Expectedly, deficiency of XRCC4 in mammalian cells caused defects in DSB repair that result in a high sensitivity to ionizing radiation (Critchlow et al. 1997). Ferguson et al. (2001) also reported that absence of *Xrcc4* in mice entailed embryonic death with a high rate of apoptosis (Ferguson and Alt 2001). On the other hand, conditional knockout of *Xrcc4* elicited aging-like phenotypes such as testicular atrophy and premature death (Li et al. 2016a). Taken together, these findings suggest that holding XRCC4 at a stable level and in an unphosphorylated state are essential processes for timely repair of DSBs by the cNHEJ pathway. Otherwise, aging-like phenotypes, cell death, and increased apoptosis may occur.

Conclusion

In this study, spatiotemporal distributions of the γH2AX, RAD51, RPA70, KU80, and XRCC4 proteins, which are involved in the DSB repair pathways, were for the first time evaluated in the postnatal mouse testes from early to aged periods. The findings suggest that changed expression of these proteins in the germinal epithelial cells of aged mice may result in increase of DSBs, likely due to decreased HR and cNHEJ repair efficiencies. Further studies are required to determine the mechanisms and factors associated with decreased levels of DSB repair proteins during testicular aging. New knowledge on this subject would contribute to developing more treatment strategies to prevent or attenuate male fertility loss that accompanies aging.

Acknowledgements We would like to thank Center for Genetic Disorders at Akdeniz University for giving permission to use the qRT-PCR machine.

Author contributions G.T. and Y.B. performed the qRT-PCR and immunohistochemistry experiments, counted the germinal epithelial cells, and analyzed all the data. G.T. wrote the manuscript, and Y.B. read it. S.O. and G.T. designed the study, and S.O. evaluated the experiment results, managed the investigation, and critically read and revised the manuscript.

Funding This study was supported by TUBITAK (project no. 219S210).

Declarations

Conflict of interest The authors declare that there is no conflict of interest that could be perceived as prejudicing the impartiality of this research.

Ethical approval All procedures performed in studies involving animals were in accordance with the ethical standards of international and national and/or institutional guidelines for the care and use of animals.

References

Agarwal A, Barbarosie C, Ambar R, Finelli R (2020) The impact of single- and double-strand DNA breaks in human spermatozoa on assisted reproduction. Int J Mol Sci. https://doi.org/10.3390/ijms21113882

Ahmed EA, van der Vaart A, Barten A, Kal HB, Chen J, Lou Z, Minter-Dykhouse K, Bartkova J, Bartek J, de Boer P, de Rooij DG (2007) Differences in DNA double strand breaks repair in male germ cell types: lessons learned from a differential expression of Mdc1 and 53BP1. DNA Repair (Amst) 6(9):1243–1254. https://doi.org/10.1016/j.dnarep.2007.02.011

Ahnesorg P, Smith P, Jackson SP (2006) XLF interacts with the XRCC4-DNA ligase IV complex to promote DNA nonhomologous end-joining. Cell 124(2):301–313. https://doi.org/10.1016/j.cell.2005.12.031

Anderson RA Jr, Phillips JF, Berryman SH, Zaneveld LJ (1989) Testosterone production by the prepubertal mouse testis is not depressed by ethanol. Reprod Toxicol 3(2):91–100

Baumann P, West SC (1998) Role of the human RAD51 protein in homologous recombination and double-stranded-break repair. Trends Biochem Sci 23(7):247–251. https://doi.org/10.1016/s0968-0004(98)01232-8

Bhasin S, Valderrabano RJ, Gagliano-Juca T. (2000) Age-related changes in the male reproductive system. In: Feingold KR, Anawalt B, Boyce A et al. (eds) Endotext, South Dartmouth (MA)

Bustin SA, Benes V, Garson JA, Hellemans J, Huggett J, Kubista M, Mueller R, Nolan T, Pfaffl MW, Shipley GL, Vandesompele J, Wittwer CT (2009) The MIQE guidelines: minimum information for publication of quantitative real-time PCR experiments. Clin Chem 55(4):611–622. https://doi.org/10.1373/clinchem.2008.112797

Chang HHY, Pannunzio NR, Adachi N, Lieber MR (2017) Non-homologous DNA end joining and alternative pathways to double-strand break repair. Nat Rev Mol Cell Biol 18(8):495–506. https://doi.org/10.1038/nrm.2017.48

Chen SR, Hao XX, Zhang Y, Deng SL, Wang ZP, Wang YQ, Wang XX, Liu YX (2016) Androgen receptor in Sertoli cells regulates DNA double-strand break repair and chromosomal synapsis of spermatocytes partially through intercellular EGF-EGFR signaling. Oncotarget 7(14):18722–18735. https://doi.org/10.18632/oncotarget.7916

Cortes-Gutierrez EI, Lopez-Fernandez C, Fernandez JL, Davila-Rodriguez MI, Johnston SD, Gosalvez J (2014) Interpreting sperm DNA damage in a diverse range of mammalian sperm by means of the two-tailed comet assay. Front Genet 5:404. https://doi.org/10.3389/fgene.2014.00404

Critchlow SE, Bowater RP, Jackson SP (1997) Mammalian DNA double-strand break repair protein XRCC4 interacts with DNA ligase IV. Curr Biol 7(8):588–598. https://doi.org/10.1016/s0960-9822(06)00258-2

Cui H, Kong Y, Zhang H (2012) Oxidative stress, mitochondrial dysfunction, and aging. J Signal Transduct 2012:646354. https://doi.org/10.1155/2012/646354

Dai J, Voloshin O, Potapova S, Camerini-Otero RD (2017) Meiotic knockdown and complementation reveals essential role of RAD51 in mouse spermatogenesis. Cell Rep 18(6):1383–1394

Duca Y, Calogero AE, Cannarella R, Condorelli RA, La Vignera S (2019) Current and emerging medical therapeutic agents for

idiopathic male infertility. Expert Opin Pharmacother 20(1):55–67. https://doi.org/10.1080/14656566.2018.1543405
Esteves SC, Miyaoka R, Agarwal AJC (2011) An update on the clinical assessment of the infertile male. Clinics (Sao Paulo) 66(4):691–700
Fell VL, Schild-Poulter C (2015) The Ku heterodimer: function in DNA repair and beyond. Mutat Res Rev Mutat Res 763:15–29. https://doi.org/10.1016/j.mrrev.2014.06.002
Ferguson DO, Alt FW (2001) DNA double strand break repair and chromosomal translocation: lessons from animal models. Oncogene 20(40):5572–5579. https://doi.org/10.1038/sj.onc.1204767
Fernandez-Gonzalez R, Moreira PN, Perez-Crespo M, Sanchez-Martin M, Ramirez MA, Pericuesta E, Bilbao A, Bermejo-Alvarez P, de Dios HJ, de Fonseca FR, Gutierrez-Adan A (2008) Long-term effects of mouse intracytoplasmic sperm injection with DNA-fragmented sperm on health and behavior of adult offspring. Biol Reprod 78(4):761–772. https://doi.org/10.1095/biolreprod.107.065623
Fix C, Jordan C, Cano P, Walker WH (2004) Testosterone activates mitogen-activated protein kinase and the cAMP response element binding protein transcription factor in Sertoli cells. Proc Natl Acad Sci USA 101(30):10919–10924. https://doi.org/10.1073/pnas.0404278101
Forand A, Dutrillaux B, Bernardino-Sgherri J (2004) Gamma-H2AX expression pattern in non-irradiated neonatal mouse germ cells and after low-dose gamma-radiation: relationships between chromatid breaks and DNA double-strand breaks. Biol Reprod 71(2):643–649. https://doi.org/10.1095/biolreprod.104.027466
Fu C, Rojas T, Chin AC, Cheng W, Bernstein IA, Albacarys LK, Wright WW, Snyder SH (2018) Multiple aspects of male germ cell development and interactions with Sertoli cells require inositol hexakisphosphate kinase-1. Sci Rep 8(1):7039. https://doi.org/10.1038/s41598-018-25468-8
Gao Y, Ferguson DO, Xie W, Manis JP, Sekiguchi J, Frank KM, Chaudhuri J, Horner J, DePinho RA, Alt FW (2000) Interplay of p53 and DNA-repair protein XRCC4 in tumorigenesis, genomic stability and development. Nature 404(6780):897–900. https://doi.org/10.1038/35009138
Gonzalez-Marin C, Gosalvez J, Roy R (2012) Types, causes, detection and repair of DNA fragmentation in animal and human sperm cells. Int J Mol Sci 13(11):14026–14052. https://doi.org/10.3390/ijms131114026
Gorbunova V, Seluanov A (2016) DNA double strand break repair, aging and the chromatin connection. Mutat Res 788:2–6. https://doi.org/10.1016/j.mrfmmm.2016.02.004
Gottlieb TM, Jackson SP (1993) The DNA-dependent protein kinase: requirement for DNA ends and association with Ku antigen. Cell 72(1):131–142. https://doi.org/10.1016/0092-8674(93)90057-w
Grabarz A, Barascu A, Guirouilh-Barbat J, Lopez BS (2012) Initiation of DNA double strand break repair: signaling and single-stranded resection dictate the choice between homologous recombination, non-homologous end-joining and alternative end-joining. Am J Cancer Res 2(3):249
Grawunder U, Wilm M, Wu X, Kulesza P, Wilson TE, Mann M, Lieber MR (1997) Activity of DNA ligase IV stimulated by complex formation with XRCC4 protein in mammalian cells. Nature 388(6641):492–495. https://doi.org/10.1038/41358
Grewenig A, Schuler N, Rube CE (2015) Persistent DNA damage in spermatogonial stem cells after fractionated low-dose irradiation of testicular tissue. Int J Radiat Oncol Biol Phys 92(5):1123–1131. https://doi.org/10.1016/j.ijrobp.2015.04.033
Gribbins KM, Elsey RM, Gist DH (2006) Cytological evaluation of the germ cell development strategy within the testis of the American alligator, *Alligator mississippiensis*. Acta Zool 87(1):59–69
Griswold MD (2016) Spermatogenesis: the commitment to meiosis. Physiol Rev 96(1):1–17. https://doi.org/10.1152/physrev.00013.2015
Gu Y, Seidl KJ, Rathbun GA, Zhu C, Manis JP, van der Stoep N, Davidson L, Cheng HL, Sekiguchi JM, Frank K, Stanhope-Baker P, Schlissel MS, Roth DB, Alt FW (1997) Growth retardation and leaky SCID phenotype of Ku70-deficient mice. Immunity 7(5):653–665. https://doi.org/10.1016/s1074-7613(00)80386-6
Gunes S, Al-Sadaan M, Agarwal A (2015) Spermatogenesis, DNA damage and DNA repair mechanisms in male infertility. Reprod Biomed Online 31(3):309–319. https://doi.org/10.1016/j.rbmo.2015.06.010
Hamer G, Roepers-Gajadien HL, van Duyn-Goedhart A, Gademan IS, Kal HB, van Buul PP, de Rooij DG (2003) DNA double-strand breaks and gamma-H2AX signaling in the testis. Biol Reprod 68(2):628–634. https://doi.org/10.1095/biolreprod.102.008672
Her J, Bunting SF (2018) How cells ensure correct repair of DNA double-strand breaks. J Biol Chem 293(27):10502–10511. https://doi.org/10.1074/jbc.TM118.000371
Hinch AG, Becker PW, Li T, Moralli D, Zhang G, Bycroft C, Green C, Keeney S, Shi Q, Davies B, Donnelly P (2020) The configuration of RPA, RAD51, and DMC1 binding in meiosis reveals the nature of critical recombination intermediates. Mol Cell 79(4):689–701. https://doi.org/10.1016/j.molcel.2020.06.015 (**e610**)
Iftode C, Daniely Y, Borowiec JA (1999) Replication protein A (RPA): the eukaryotic SSB. Crit Rev Biochem Mol Biol 34(3):141–180. https://doi.org/10.1080/10409239991209255
Jean-Faucher C, Berger M, de Turckheim M, Veyssiere G, Jean C (1978) Developmental patterns of plasma and testicular testosterone in mice from birth to adulthood. Acta Endocrinol (Copenh) 89(4):780–788. https://doi.org/10.1530/acta.0.0890780
Ji G, Gu A, Wang Y, Huang C, Hu F, Zhou Y, Song L, Wang X (2012) Genetic variants in antioxidant genes are associated with sperm DNA damage and risk of male infertility in a Chinese population. Free Radic Biol Med 52(4):775–780
Johnson L, Zane RS, Petty CS, Neaves WB (1984) Quantification of the human Sertoli cell population: its distribution, relation to germ cell numbers, and age-related decline. Biol Reprod 31(4):785–795. https://doi.org/10.1095/biolreprod31.4.785
Kamel D, Mackey ZB, Sjöblom T, Walter CA, McCarrey JR, Uitto L, Palosaari H, Lähdetie J, Tomkinson AE, Syväoja JE (1997) Role of deoxyribonucleic acid polymerase ε in spermatogenesis in mice. Biol Reprod 57(6):1367–1374
Khanna KK, Jackson SP (2001) DNA double-strand breaks: signaling, repair and the cancer connection. Nat Genet 27(3):247–254
Kinner A, Wu W, Staudt C, Iliakis G (2008) Gamma-H2AX in recognition and signaling of DNA double-strand breaks in the context of chromatin. Nucleic Acids Res 36(17):5678–5694. https://doi.org/10.1093/nar/gkn550
Kosebent EG, Ozturk S (2021a) The spatiotemporal expression of TERT and telomere repeat binding proteins in the postnatal mouse testes. Andrologia 53(3):e13976. https://doi.org/10.1111/and.13976
Kosebent EG, Ozturk S (2021b) Telomere associated gene expression as well as TERT protein level and telomerase activity are altered in the ovarian follicles of aged mice. Sci Rep 11(1):15569. https://doi.org/10.1038/s41598-021-95239-5
Kotaja N, Kimmins S, Brancorsini S, Hentsch D, Vonesch JL, Davidson I, Parvinen M, Sassone-Corsi P (2004) Preparation, isolation and characterization of stage-specific spermatogenic cells for cellular and molecular analysis. Nat Methods 1(3):249–254. https://doi.org/10.1038/nmeth1204-249
Kuo LJ, Yang L-X (2008) γ-H2AX-a novel biomarker for DNA double-strand breaks. In Vivo 22(3):305–309
Kuramochi-Miyagawa S, Kimura T, Ijiri TW, Isobe T, Asada N, Fujita Y, Ikawa M, Iwai N, Okabe M, Deng W, Lin H, Matsuda Y, Nakano T (2004) Mili, a mammalian member of piwi family gene, is essential for spermatogenesis. Development 131(4):839–849. https://doi.org/10.1242/dev.00973

Lam I, Keeney S (2014) Mechanism and regulation of meiotic recombination initiation. Cold Spring Harb Perspect Biol 7(1):a016634. https://doi.org/10.1101/cshperspect.a016634

Li X, Heyer WD (2008) Homologous recombination in DNA repair and DNA damage tolerance. Cell Res 18(1):99–113. https://doi.org/10.1038/cr.2008.1

Li T, Liu X, Jiang L, Manfredi J, Zha S, Gu W (2016a) Loss of p53-mediated cell-cycle arrest, senescence and apoptosis promotes genomic instability and premature aging. Oncotarget 7(11):11838–11849. https://doi.org/10.18632/oncotarget.7864

Li Z, Zhang W, Chen Y, Guo W, Zhang J, Tang H, Xu Z, Zhang H, Tao Y, Wang F, Jiang Y, Sun FL, Mao Z (2016b) Impaired DNA double-strand break repair contributes to the age-associated rise of genomic instability in humans. Cell Death Differ 23(11):1765–1777. https://doi.org/10.1038/cdd.2016.65

Lombard DB, Chua KF, Mostoslavsky R, Franco S, Gostissa M, Alt FW (2005) DNA repair, genome stability, and aging. Cell 120(4):497–512

Marini F, Rawal CC, Liberi G, Pellicioli A (2019) Regulation of DNA double strand breaks processing: focus on barriers. Front Mol Biosci 6:55. https://doi.org/10.3389/fmolb.2019.00055

Meistrich ML, Hess RA (2013) Assessment of spermatogenesis through staging of seminiferous tubules. Methods Mol Biol 927:299–307. https://doi.org/10.1007/978-1-62703-038-0_27

Meistrich ML, Bruce WR, Clermont Y (1973) Cellular composition of fractions of mouse testis cells following velocity sedimentation separation. Exp Cell Res 79(1):213–227

Muratori M, Marchiani S, Tamburrino L, Baldi E (2019) Sperm DNA fragmentation: mechanisms of origin. Adv Exp Med Biol 1166:75–85. https://doi.org/10.1007/978-3-030-21664-1_5

Neaves WB, Johnson L, Porter JC, Parker CR Jr, Petty CS (1984) Leydig cell numbers, daily sperm production, and serum gonadotropin levels in aging men. J Clin Endocrinol Metab 59(4):756–763. https://doi.org/10.1210/jcem-59-4-756

Neaves WB, Johnson L, Petty CS (1985) Age-related change in numbers of other interstitial cells in testes of adult men: evidence bearing on the fate of Leydig cells lost with increasing age. Biol Reprod 33(1):259–269. https://doi.org/10.1095/biolreprod33.1.259

Nguyen-Powanda P, Robaire B (2021) Aging and oxidative stress alter DNA repair mechanisms in male germ cells of superoxide dismutase-1 null mice. Biol Reprod 105(4):944–957. https://doi.org/10.1093/biolre/ioab114

O'Donnell L (2014) Mechanisms of spermiogenesis and spermiation and how they are disturbed. Spermatogenesis 4(2):e979623. https://doi.org/10.4161/21565562.2014.979623

Ouyang H, Nussenzweig A, Kurimasa A, Soares VC, Li X, Cordon-Cardo C, Li W, Cheong N, Nussenzweig M, Iliakis G, Chen DJ, Li GC (1997) Ku70 is required for DNA repair but not for T cell antigen receptor gene recombination In vivo. J Exp Med 186(6):921–929. https://doi.org/10.1084/jem.186.6.921

Ozturk S, Guzeloglu-Kayisli O, Demir N, Sozen B, Ilbay O, Lalioti MD, Seli E (2012) Epab and Pabpc1 are differentially expressed during male germ cell development. Reprod Sci 19(9):911–922. https://doi.org/10.1177/1933719112446086

Ozturk S, Guzeloglu-Kayisli O, Lowther KM, Lalioti MD, Sakkas D, Seli E (2014) Epab is dispensable for mouse spermatogenesis and male fertility. Mol Reprod Dev 81(5):390. https://doi.org/10.1002/mrd.22319

Pandey M, Raghavan SC (2017) DNA double-strand break repair in mammals. J Radiat Cancer Res 8(2):93

Paniagua R, Nistal M, Saez FJ, Fraile B (1991) Ultrastructure of the aging human testis. J Electron Microsc Tech 19(2):241–260. https://doi.org/10.1002/jemt.1060190209

Pannunzio NR, Watanabe G, Lieber MR (2018) Nonhomologous DNA end-joining for repair of DNA double-strand breaks. J Biol Chem 293(27):10512–10523. https://doi.org/10.1074/jbc.TM117.000374

Parada-Bustamante A, Molina C, Valencia C, Florez M, Lardone MC, Argandona F, Piottante A, Ebensperguer M, Orihuela PA, Castro A (2017) Disturbed testicular expression of the estrogen-metabolizing enzymes CYP1A1 and COMT in infertile men with primary spermatogenic failure: possible negative implications on Sertoli cells. Andrology 5(3):486–494. https://doi.org/10.1111/andr.12346

Paul C, Robaire B (2013) Ageing of the male germ line. Nat Rev Urol 10(4):227–234. https://doi.org/10.1038/nrurol.2013.18

Paul C, Nagano M, Robaire B (2013) Aging results in molecular changes in an enriched population of undifferentiated rat spermatogonia. Biol Reprod 89(6):147. https://doi.org/10.1095/biolreprod.113.112995

Qu W, Liu C, Xu YT, Xu YM, Luo MC (2021) The formation and repair of DNA double-strand breaks in mammalian meiosis. Asian J Androl 23(6):572–579. https://doi.org/10.4103/aja202191

Robert N, Yan C, Si-Jiu Y, Bo L, He H, Pengfei Z, Hongwei X, Jian Z, Shijie L, Qian Z (2021) Expression of Rad51 and the histomorphological evaluation of testis of the sterile male cattle-yak. Theriogenology 172:239–254. https://doi.org/10.1016/j.theriogenology.2021.06.018

Rosiak-Gill A, Gill K, Jakubik J, Fraczek M, Patorski L, Gaczarzewicz D, Kurzawa R, Kurpisz M, Piasecka MJA (2019) Age-related changes in human sperm DNA integrity. Aging (Albany NY) 11(15):5399

Santiago J, Silva JV, Alves MG, Oliveira PF, Fardilha M (2019) Testicular aging: an overview of ultrastructural, cellular, and molecular alterations. J Gerontol A Biol Sci Med Sci 74(6):860–871. https://doi.org/10.1093/gerona/gly082

Scully R, Panday A, Elango R, Willis NA (2019) DNA double-strand break repair-pathway choice in somatic mammalian cells. Nat Rev Mol Cell Biol 20(11):698–714. https://doi.org/10.1038/s41580-019-0152-0

Sellou H, Lebeaupin T, Chapuis C, Smith R, Hegele A, Singh HR, Kozlowski M, Bultmann S, Ladurner AG, Timinszky G, Huet S (2016) The poly(ADP-ribose)-dependent chromatin remodeler Alc1 induces local chromatin relaxation upon DNA damage. Mol Biol Cell 27(24):3791–3799. https://doi.org/10.1091/mbc.E16-05-0269

Shi B, Xue J, Yin H, Guo R, Luo M, Ye L, Shi Q, Huang X, Liu M, Sha J, Wang PJ (2019) Dual functions for the ssDNA-binding protein RPA in meiotic recombination. PLoS Genet 15(2):e1007952. https://doi.org/10.1371/journal.pgen.1007952

Singh NP, Muller CH, Berger RE (2003) Effects of age on DNA double-strand breaks and apoptosis in human sperm. Fertil Steril 80(6):1420–1430. https://doi.org/10.1016/j.fertnstert.2003.04.002

Snyder PJ (2001) Effects of age on testicular function and consequences of testosterone treatment. J Clin Endocrinol Metab 86(6):2369–2372. https://doi.org/10.1210/jcem.86.6.7602

Soutoglou E, Dorn JF, Sengupta K, Jasin M, Nussenzweig A, Ried T, Danuser G, Misteli T (2007) Positional stability of single double-strand breaks in mammalian cells. Nat Cell Biol 9(6):675–682. https://doi.org/10.1038/ncb1591

Stinson BM, Moreno AT, Walter JC, Loparo JJ (2020) A mechanism to minimize errors during non-homologous end joining. Mol Cell 77(5):1080–1091. https://doi.org/10.1016/j.molcel.2019.11.018 (**e1088**)

Sung P, Klein H (2006) Mechanism of homologous recombination: mediators and helicases take on regulatory functions. Nat Rev Mol Cell Biol 7(10):739–750

Sung P, Krejci L, Van Komen S, Sehorn MG (2003) Rad51 recombinase and recombination mediators. J Biol Chem 278(44):42729–42732. https://doi.org/10.1074/jbc.R300027200

Talibova G, Bilmez Y, Ozturk S (2022) DNA double-strand break repair in male germ cells during spermatogenesis and its association with male infertility development. DNA Repair (Amst) 118:103386. https://doi.org/10.1016/j.dnarep.2022.103386

Tenover JS (2003) Declining testicular function in aging men. Int J Impot Res 15(Suppl 4):S3-8. https://doi.org/10.1038/sj.ijir.3901029

Tepekoy F, Ozturk S, Sozen B, Ozay RS, Akkoyunlu G, Demir N (2015) CD90 and CD105 expression in the mouse ovary and testis at different stages of postnatal development. Reprod Biol 15(4):195–204. https://doi.org/10.1016/j.repbio.2015.10.004

Terasawa M, Shinohara A, Shinohara M (2014) Canonical non-homologous end joining in mitosis induces genome instability and is suppressed by M-phase-specific phosphorylation of XRCC4. PLoS Genet 10(8):e1004563. https://doi.org/10.1371/journal.pgen.1004563

Tesarik J, Greco E, Mendoza C (2004) Late, but not early, paternal effect on human embryo development is related to sperm DNA fragmentation. Hum Reprod 19(3):611–615. https://doi.org/10.1093/humrep/deh127

Turinetto V, Giachino C (2015) Multiple facets of histone variant H2AX: a DNA double-strand-break marker with several biological functions. Nucleic Acids Res 43(5):2489–2498. https://doi.org/10.1093/nar/gkv061

Um JH, Kim SJ, Kim DW, Ha MY, Jang JH, Kim DW, Chung BS, Kang CD, Kim SH (2003) Tissue-specific changes of DNA repair protein Ku and mtHSP70 in aging rats and their retardation by caloric restriction. Mech Ageing Dev 124(8–9):967–975. https://doi.org/10.1016/s0047-6374(03)00169-6

Uysal F, Ozturk S (2020) The loss of global DNA methylation due to decreased DNMT expression in the postnatal mouse ovaries may associate with infertility emerging during ovarian aging. Histochem Cell Biol 154(3):301–314. https://doi.org/10.1007/s00418-020-01890-w

Vaidya A, Mao Z, Tian X, Spencer B, Seluanov A, Gorbunova V (2014) Knock-in reporter mice demonstrate that DNA repair by non-homologous end joining declines with age. PLoS Genet 10(7):e1004511

Vasco C, Zuccotti M, Redi CA, Garagna S (2009) Identification, isolation, and RT-PCR analysis of single stage-specific spermatogenetic cells obtained from portions of seminiferous tubules classified by transillumination microscopy. Mol Reprod Dev 76(12):1173–1177. https://doi.org/10.1002/mrd.21086

Walker WH (2010) Non-classical actions of testosterone and spermatogenesis. Philos Trans R Soc Lond B Biol Sci 365(1546):1557–1569. https://doi.org/10.1098/rstb.2009.0258

Whelan DR, Lee WTC, Yin Y, Ofri DM, Bermudez-Hernandez K, Keegan S, Fenyo D, Rothenberg E (2018) Spatiotemporal dynamics of homologous recombination repair at single collapsed replication forks. Nat Commun 9(1):3882. https://doi.org/10.1038/s41467-018-06435-3

Wolf KN, Wildt DE, Vargas A, Marinari PE, Kreeger JS, Ottinger MA, Howard JG (2000) Age-dependent changes in sperm production, semen quality, and testicular volume in the black-footed ferret (*Mustela nigripes*). Biol Reprod 63(1):179–187. https://doi.org/10.1095/biolreprod63.1.179

Yates LA, Aramayo RJ, Pokhrel N, Caldwell CC, Kaplan JA, Perera RL, Spies M, Antony E, Zhang X (2018) A structural and dynamic model for the assembly of Replication Protein A on single-stranded DNA. Nat Commun 9(1):5447. https://doi.org/10.1038/s41467-018-07883-7

Yuan J, Adamski R, Chen J (2010) Focus on histone variant H2AX: to be or not to be. FEBS Lett 584(17):3717–3724

Zou Y, Liu Y, Wu X, Shell SM (2006) Functions of human replication protein A (RPA): from DNA replication to DNA damage and stress responses. J Cell Physiol 208(2):267–273. https://doi.org/10.1002/jcp.20622